

Orcina project 1429

OrcaWave validation report

Orcina Ltd.

Daltongate
Ulverston
Cumbria
LA12 7AJ
United Kingdom

E: orcina@orcina.com

T: +44 (0)1229 584 742

Client:	N/A			
Revision History:	Report No.	Issue	Report Date	Report Status
	01	01	20/03/2020	Issued
For Orcina:	Author:	C. Heaton	<i>C. J. Heaton</i>	
	Checked:	D. Heffernan	<i>D. Heffernan</i>	
Report file:				

CONTENTS

1.	Introduction	3
1.1.	Abbreviations	3
1.2.	Symbols	3
1.3.	Units.....	4
1.4.	References	4
2.	First-order validation cases	5
2.1.	Vertical circular cylinder.....	5
2.2.	Vertical circular cylinder with irregular frequency removal	9
2.3.	Heeled circular cylinder	14
2.4.	Floating hemisphere.....	18
2.5.	ISSC tension leg platform.....	21
2.6.	Multibody analysis of a circular cylinder and ellipsoid	26
2.7.	Inverted pyramid with control surface mean drift loads	28
2.8.	Ellipsoid with control surface mean drift load	33
2.9.	Circular cylinder with moonpool and damping lid	37
3.	Second-order validation cases.....	40
3.1.	QTFs of a bottom-mounted circular cylinder	40
3.2.	QTFs of a floating hemisphere in shallow water	43
3.3.	Multibody QTF analysis of a circular cylinder and ellipsoid	47

1. Introduction

OrcaWave is a diffraction analysis program which calculates loading and response for wet bodies due to surface water waves via potential flow theory. This major new area of functionality was introduced to OrcaFlex version 11.0 in November 2019.

We have validated OrcaWave by comparing its results to theoretical predictions where possible, e.g. for a floating hemisphere (Section 2.4) and a bottom-mounted circular cylinder (Section 3.1). However, analytic results are only available for a very few simple geometries.

More comprehensive validation has been performed by comparing results from OrcaWave to results from Wamit. The majority of this report is concerned with describing the validation we have performed against Wamit, using a set of test cases that cover the entire range of functionality of OrcaWave.

For each of the validation cases described in this report you can download model files to run the analysis yourself in OrcaWave and/or Wamit. In this report we have used the latest versions of both programs: OrcaWave v11.0, Wamit v7.31 for first-order analysis (i.e. throughout Section 2) and Wamit v6.43S for second-order analysis (i.e. throughout Section 3).

Inevitably, some judgement is needed to select consistent options and settings when running the same model in two different computer programs. We have tried to choose the most consistent settings possible. For example, all our Wamit models use `ILOG=1` to be consistent with how OrcaWave handles the logarithmic singularity in the Green's function. However, in some cases the choice is less clear-cut. If you think one of the validation cases in this report can be improved in any way please do let us know via orcina@orcina.com.

1.1. Abbreviations

Abbreviation	Description
RAO	Response amplitude operator
QTF	Quadratic transfer function
CAD	Computer-aided design
ISSC	International ship and offshore structures congress
TLP	Tension-leg platform
PI	Pressure integration method for mean drift loads and quadratic loads (also known as the near-field method)
CS	Control surface method for mean drift loads and quadratic loads (also known as the middle-field method)

Table 1 – List of Abbreviations

1.2. Symbols

Symbol	Description
ω	Wave angular frequency
T	Wave period
β	Wave heading

Table 2 – List of Symbols

1.3. Units

Unit	Description
%	Percent
deg ($^{\circ}$)	Degree
m	Metre
rad	Radian
s	Second

Table 3 – List of Units

1.4. References

No.	
1.	Orcina Ltd, 2019, <i>OrcaWave documentation</i> . www.orcina.com/webhelp/OrcaWave .
2.	Wamit Inc., 2019, <i>The Wamit user manual, version 7.3</i> . www.wamit.com/manual.htm .
3.	Wamit Inc., 2019, <i>The Wamit user manual, version 6.4S</i> . www.wamit.com/manual6.htm .
4.	Malenica, S., Chen, X.B., 1998, <i>On the irregular frequencies appearing in wave diffraction-radiation solutions</i> . Int. J. Offshore Polar., 8 : 110–114.
5.	Hulme, A., 1982, <i>The wave forces acting on a floating hemisphere undergoing forced periodic oscillations</i> , J. Fluid Mech., 121 : 443–463.
6.	Eatock Taylor, R., Jeffreys, E.R., 1986, <i>Variability of hydrodynamic load predictions for a tension leg platform</i> . Ocean Eng., 13 : 449—490.
7.	Chen, X-B, 2004, <i>Hydrodynamics in Offshore and Naval Applications – Part I</i> . 6th International Conference on Hydrodynamics, Perth.
8.	Chen, X-B, 2007, <i>Middle-field formulation for the computation of drift loads</i> . J. Eng. Math., 59 : 61—82.
9.	Eatock Taylor, R., Hung, S.M., 1987, <i>Second order diffraction forces on a vertical cylinder in regular waves</i> , Appl. Ocean Res., 9 : 19–30.

Table 4 – List of References

2. First-order validation cases

2.1. Vertical circular cylinder

2.1.1. Description

This case is based on the TEST01 case of the Wamit v7.3 program. The body is a freely-floating vertical cylinder of radius 1m and draught 0.5m. The water depth is infinite. The body mesh has two planes of symmetry, with the file test01.gdf having 256 panels to describe one quadrant of the body. Wave headings of $\beta = 0^\circ$ and 27° and a range of wave frequencies $0.1 \leq \omega \leq 5$ rad/s are considered.

The choice of wave frequencies is influenced by the mesh, specifically the fact that it does not include panels on the interior free surface to remove the effects of irregular frequencies. OrcaWave estimates that the first irregular frequency will occur at $\omega \approx 5.2$ rad/s (and will issue a warning if a higher frequency is analysed without extending the mesh, see [1]). In fact, for this simple geometry the irregular frequencies are known analytically [4] and their values are $\omega = 5.32, 6.26, 7.14, 7.39, 7.92, 8.30, 8.63, 9.09 \dots$ rad/s.

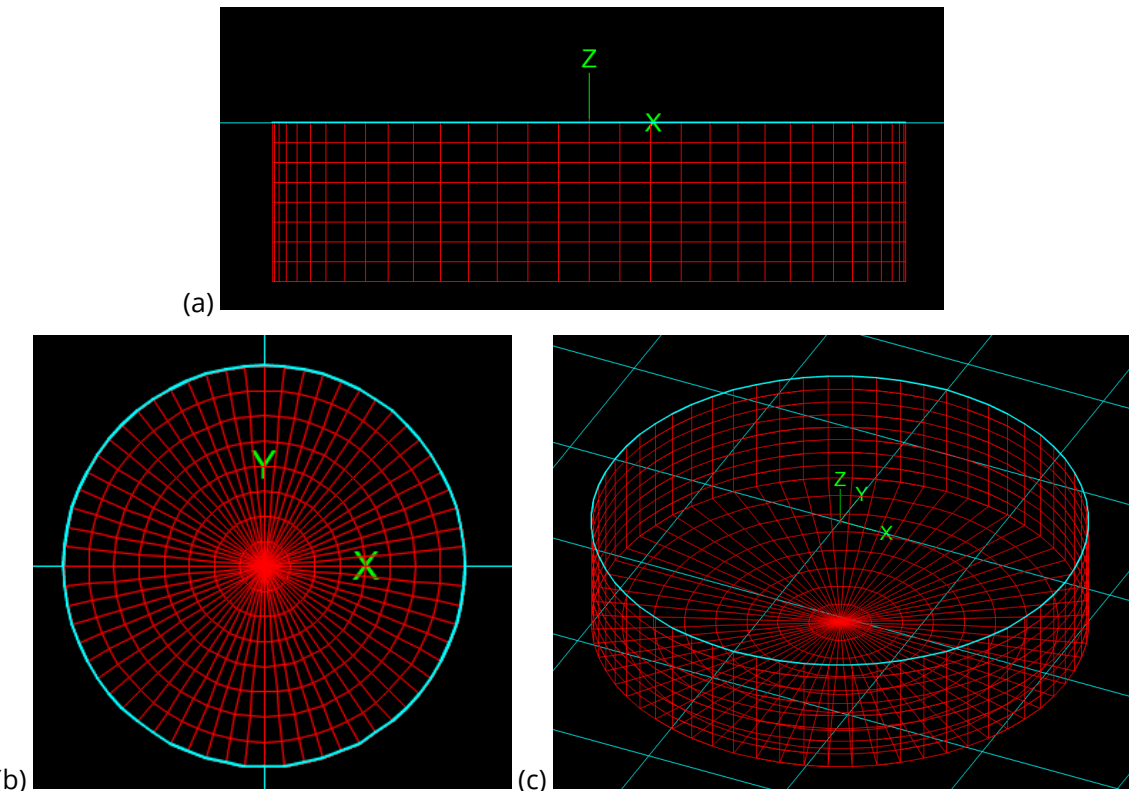


Figure 1. Elevation (a), plan (b) and perspective (c) views of the body mesh for test01.gdf.

2.1.2. Results

OrcaWave results show excellent agreement with Wamit over the range of wave frequencies considered $0.1 \leq \omega \leq 5$ rad/s. For example, Figure 2 shows the comparison of the Haskind load RAOs in each degree of freedom and Figure 3 shows the PI mean drift load. In these figures, and throughout this report, we have plotted the dimensional results that are reported by OrcaWave. Dimensional Wamit results are obtained by taking the non-dimensional results reported by the program and multiplying by the appropriate factors given in the Wamit user manual [2].

Comparisons have also been made for the added and damping matrices, diffraction load RAOs, displacement RAOs and sea state RAOs. For brevity, plots of each result quantity are not included in this report, but note that the OrcaWave and Wamit input files are available to download to accompany this report.

The results from both OrcaWave and Wamit show a small blip in the heave component of mean drift load (Figure 3) at $\omega \approx 1.5$ rad/s. This corresponds to a parametric roll resonance¹. At this frequency the forces on the body are regular (see Figure 2) but the resonance causes relatively large amplitude motion in roll/pitch which can be seen in the displacement RAOs and, indirectly, in the mean drift loads. This cylindrical vessel is only a validation case therefore we do not seek to address this. However, real-world vessel shapes can also display roll resonances, with potential theory typically overestimating the motion because it neglects viscous damping. In such situations it is common to add an external damping matrix to the body to improve the agreement with measured data.

2.1.3. Further considerations

The wave frequencies considered for this case were chosen to avoid any irregular frequency effects. We study higher frequency waves interacting with the same body in Section 2.2, using an extended mesh to demonstrate the removal of irregular frequency effects.

¹N.B. since the body is axisymmetric it could equally be called a parametric pitch resonance.

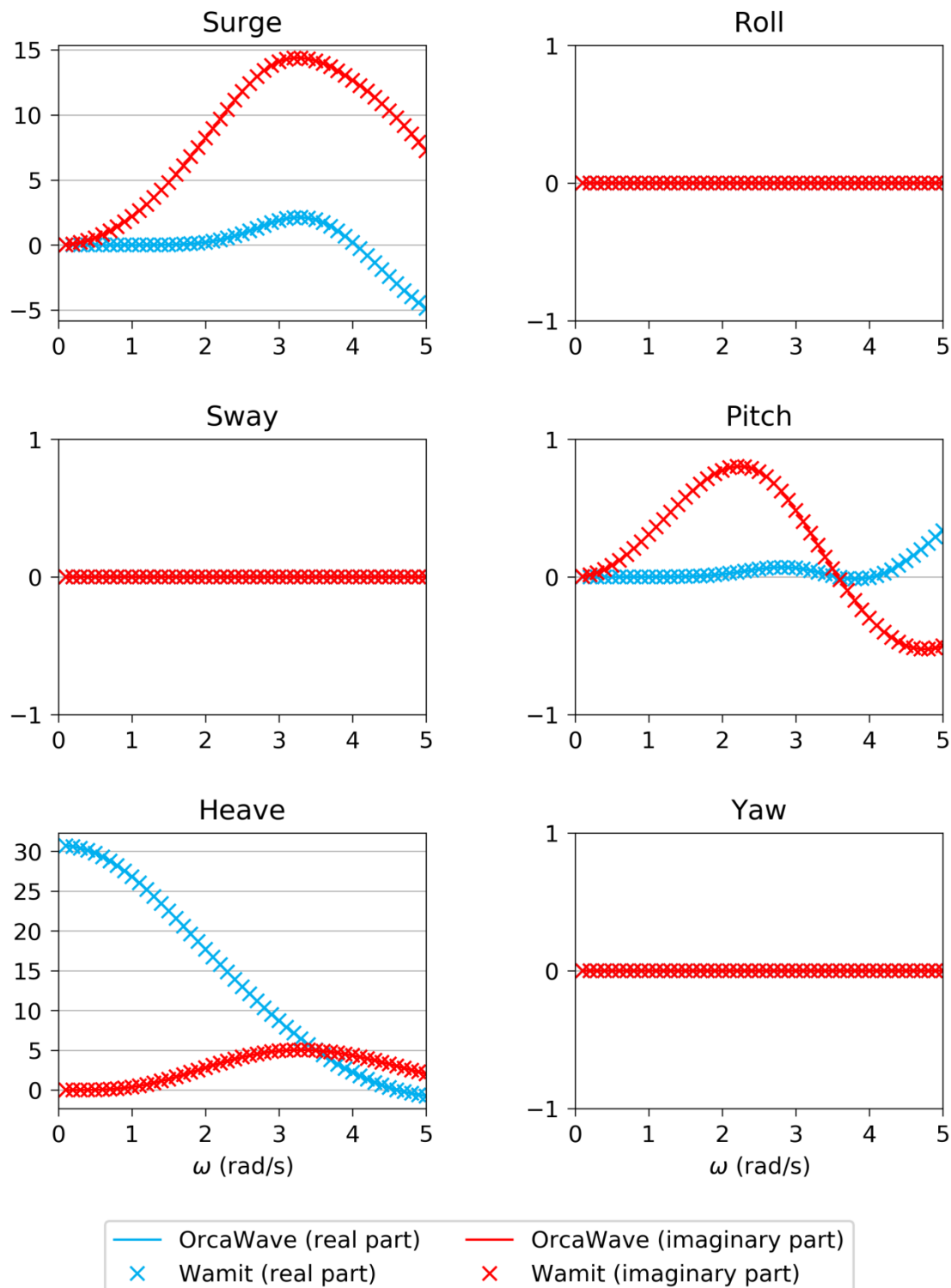


Figure 2. Haskind load RAOs for $\beta = 0^\circ$. The horizontal axes are angular frequency (rad/s). The vertical axis is kN/m for surge, sway and heave, kN.m/m for roll, pitch and yaw.

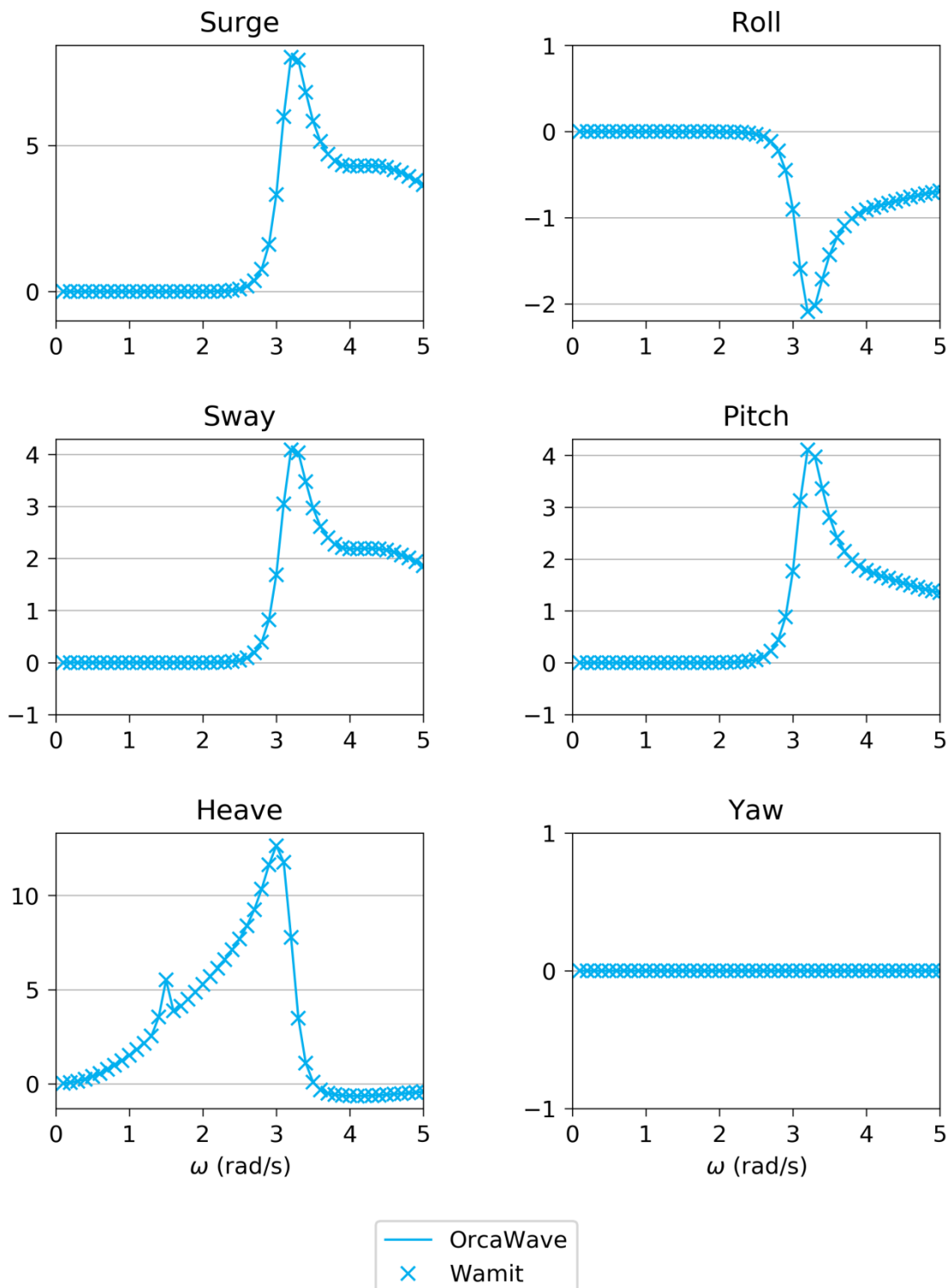


Figure 3. PI mean drift loads for $\beta = 27^\circ$. The horizontal axes are angular frequency (rad/s). The vertical axis is kN/m^2 for surge, sway and heave, kN.m/m^2 for roll, pitch and yaw.

2.2. Vertical circular cylinder with irregular frequency removal

2.2.1. Description

This case is based on the TEST01b case of the Wamit v7.3 program. The body is the same freely-floating vertical cylinder as Section 2.1 and the water depth is again infinite. Wave headings of $\beta = 0^\circ$ and 27° and a range of wave frequencies $0.1 \leq \omega \leq 10$ rad/s are considered.

The body mesh must be extended to include panels on the interior free surface in order to remove the effects of irregular frequencies. We use the same body mesh file as Section 2.1 and select the option for OrcaWave to automatically add interior surface panels. Alternatively, for full control over the mesh design, we could draw an extended mesh in a CAD program and export a mesh file for use in OrcaWave. Using a CAD program may be beneficial for more complicated geometries, but for this case the automatic procedure is sufficient.

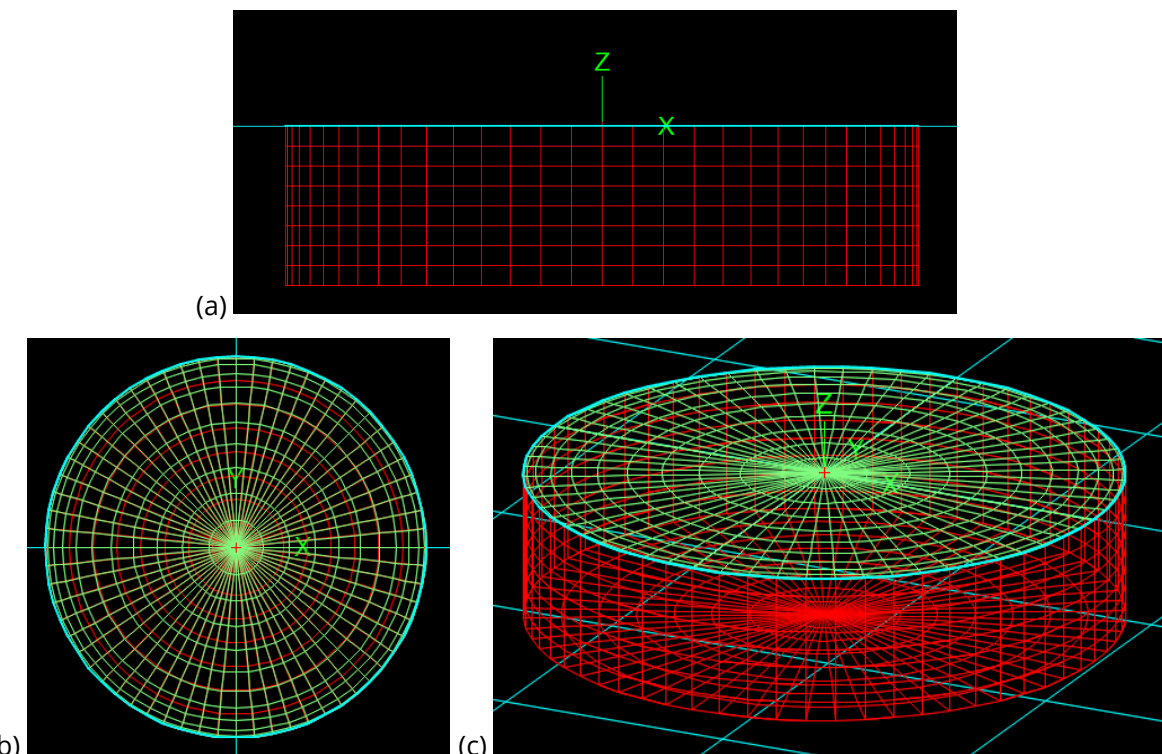


Figure 4. Elevation (a), plan (b) and perspective (c) views of the body mesh from test01.gdf (red) and the additional panels on the interior free surface (green).

2.2.2. Results

OrcaWave results again show excellent agreement with Wamit over the range of wave frequencies considered $0.1 \leq \omega \leq 10$ rad/s. Figure 5 and Figure 6 show the Haskind load RAOs and PI mean drift loads, the same result quantities as were presented in Section 2.1.

The results shown in the figures are smooth for the higher frequencies $\omega > 5$ introduced in this case, indicating that the effects of the irregular frequencies have been successfully removed. Irregular frequency effects, when present, are usually seen as spikes and discontinuities when results are plotted against wave frequency (or period). To demonstrate the importance of removing them, Figure 7 shows the results for the surge component of PI mean drift force if the mesh is not extended.

2.2.3. Further considerations

The theory underlying the removal of irregular frequency effects ensures that the process of extending the mesh does not have undesired effects on the results at regular wave frequencies. This is demonstrated in Figure 8, which shows that the OrcaWave results are unchanged in the range of regular frequencies, $\omega \leq 5$.

Extending the mesh does have the drawback that it increases the size of the mesh and therefore increases the run time of the calculation. If an analysis only requires wave frequencies which are less than the first irregular frequency, it is therefore preferable to use a mesh of the hull alone.

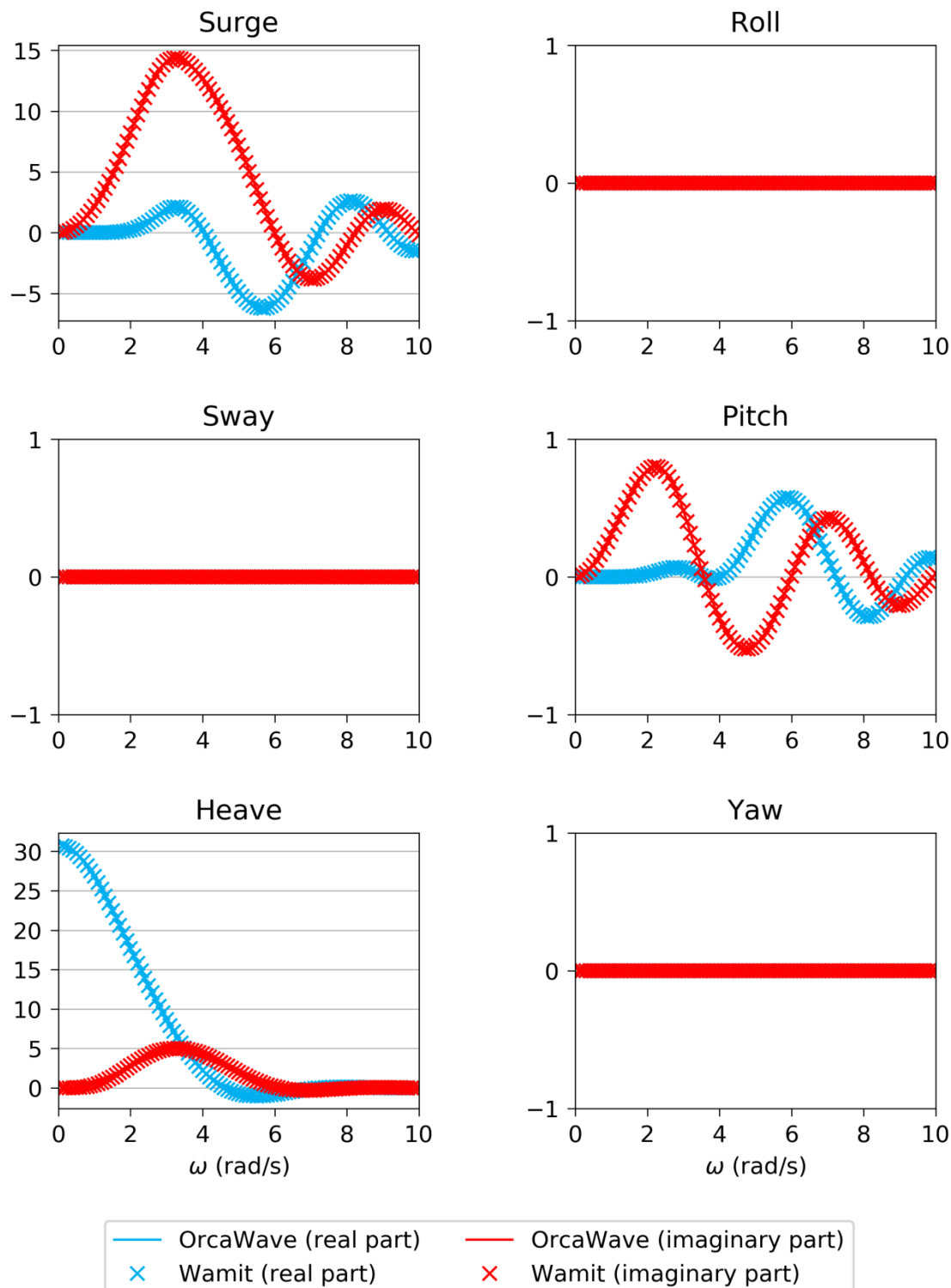


Figure 5. Haskind load RAOs for $\beta = 0^\circ$. The horizontal axes are angular frequency (rad/s). The vertical axis is kN/m for surge, sway and heave, kN.m/m for roll, pitch and yaw.

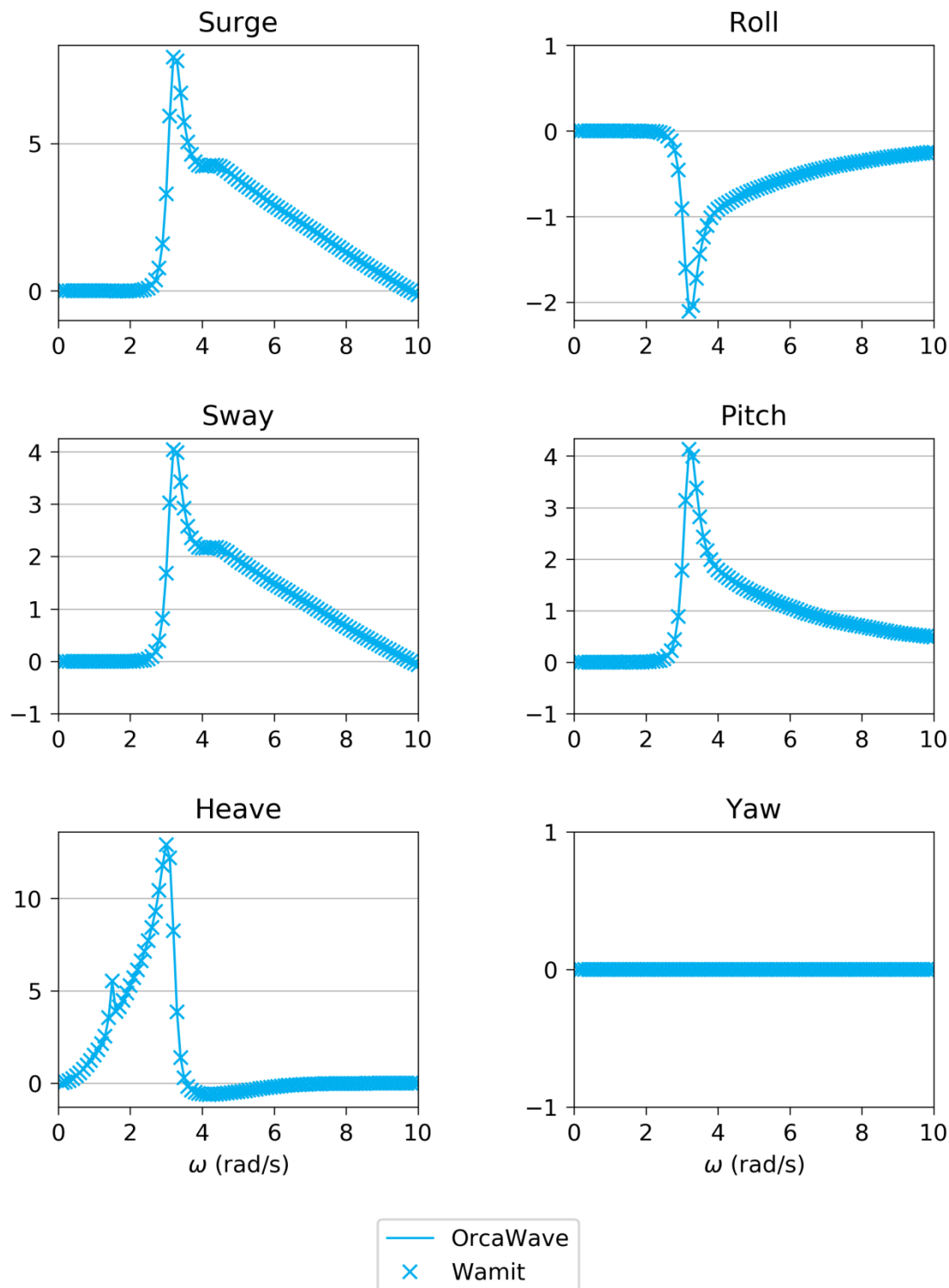


Figure 6. PI mean drift loads for $\beta = 27^\circ$. The horizontal axes are angular frequency (rad/s). The vertical axis is kN/m² for surge, sway and heave, kN.m/m² for roll, pitch and yaw.

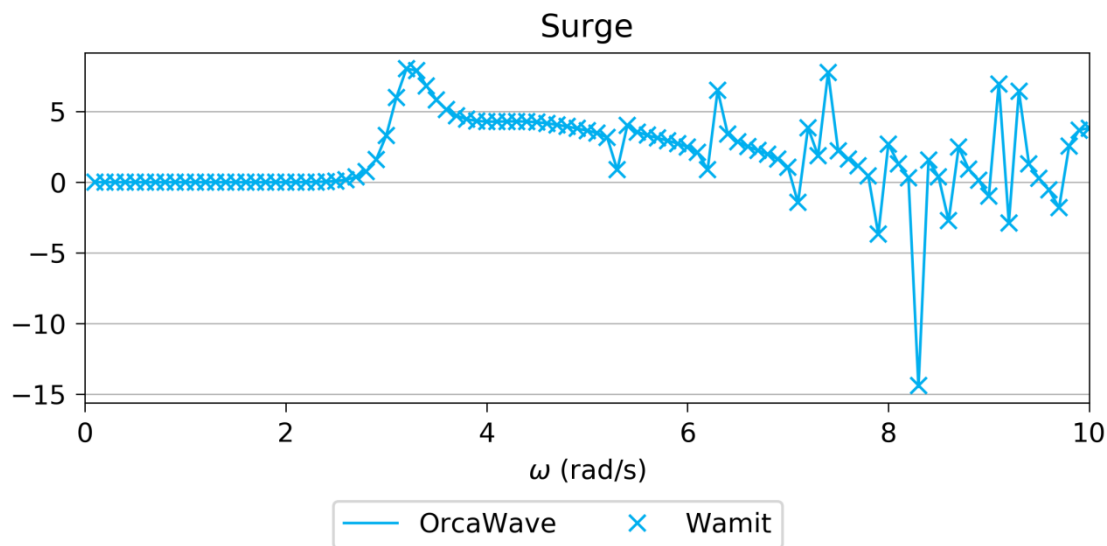


Figure 7. The surge component of PI mean drift force for $\beta = 27^\circ$, demonstrating irregular frequency effects when the mesh is not extended. The horizontal axis is angular frequency (rad/s). The vertical axis is kN/m².

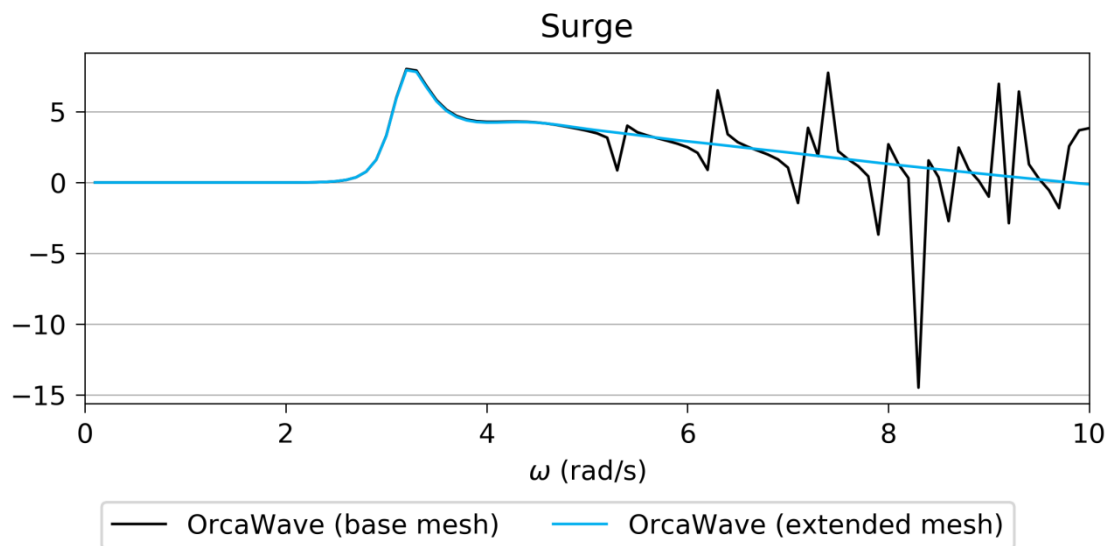


Figure 8. The surge component of PI mean drift force for $\beta = 27^\circ$, demonstrating the removal of irregular frequency effects at higher ω , whilst leaving results unchanged at lower ω . The horizontal axis is angular frequency (rad/s). The vertical axis is kN/m².

2.3. Heeled circular cylinder

2.3.1. Description

This case is based on the TEST01a case of the Wamit v7.3 program. The body is the same cylinder as Section 2.1, but with a different orientation and position: the mesh has a heel angle of 15° and the mesh origin is raised 0.27m above the free surface of the water. The water depth is again infinite.

One approach to study this body in OrcaWave would be to create a new mesh file using a CAD program. However, instead we use the same body mesh file, test01.gdf, as in Section 2.1 and set the mesh position and mesh orientation to the above values. OrcaWave automatically rotates and translates the mesh to the specified position and orientation, as well as clipping the mesh at the free surface.

Figure 9 shows the resulting mesh. Dry panels are shown in grey: they have been clipped from the mesh and do not participate in the calculation, but are shown for illustration.

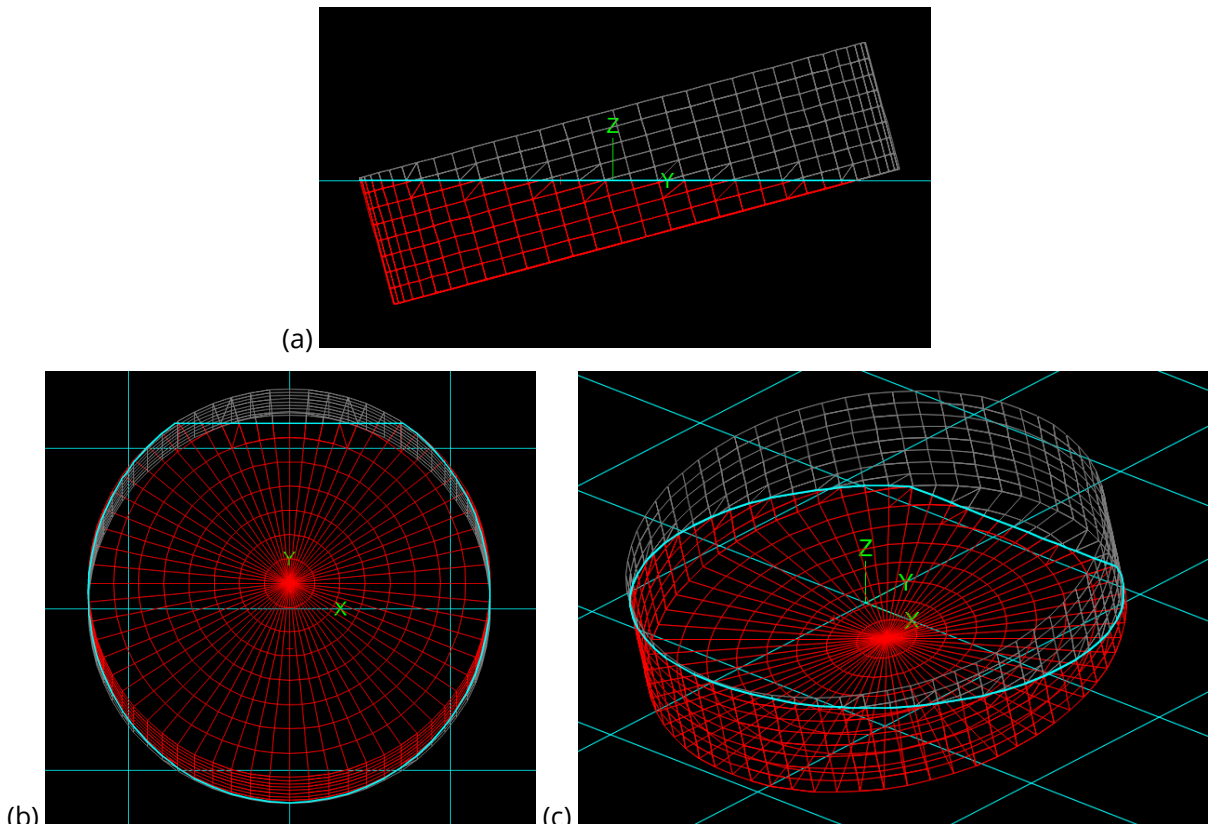


Figure 9. Elevation (a), plan (b) and perspective (c) views of the body mesh for the heeled circular cylinder.

2.3.2. Results

The agreement between OrcaWave and Wamit is shown in Figure 10 for Haskind load RAOs and, for variety, Figure 11 shows results for a sea state RAO.

This body again has a parametric roll resonance, now at $\omega \approx 2.6$ rad/s. As in Section 2.1, the load RAOs (Figure 10) and the added mass and damping matrices (not shown) vary smoothly as ω passes through this frequency, but the resonance causes a singularity in displacement RAO

values. Sea state RAOs, as well as mean drift loads and all second-order loads, depend on the displacement RAOs and therefore the results in Figure 11 show an effect of the roll resonance. For this rather artificial validation case we do not address the resonance, but for a real-world vessel it is usual to add an external damping matrix to the body to improve the agreement between potential theory and measured data.

2.3.3. Further considerations

Although the body mesh file test01.gdf has two planes of symmetry, Figure 9 shows that symmetry in the XZ plane is lost by rotating it to a heel angle of 15°. The calculation mesh for this case has only one symmetry plane (YZ), and as a consequence the calculations take noticeably longer to complete than Section 2.1.

The first irregular frequency is estimated at $\omega \approx 5.3$ rad/s for this body. For simplicity we have considered wave frequencies $0.1 \leq \omega \leq 5$ rad/s to avoid complicating the presentation. Higher wave frequencies can be analysed in the same way as Section 2.2 by extending the mesh to include the interior free surface.

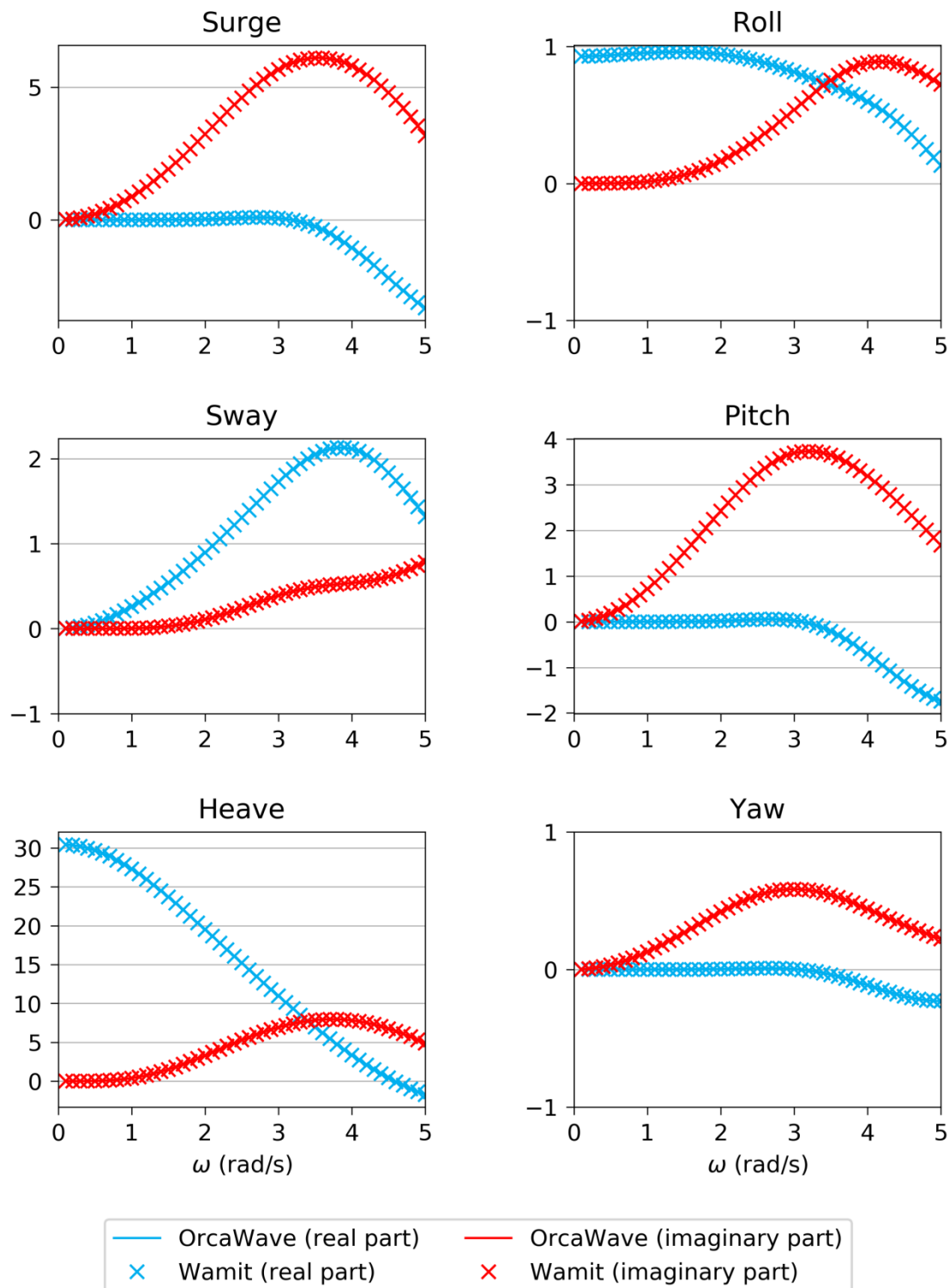


Figure 10. Haskind load RAOs for $\beta = 0^\circ$. The horizontal axes are angular frequency (rad/s). The vertical axis is kN/m for surge, sway and heave, kN.m/m for roll, pitch and yaw.

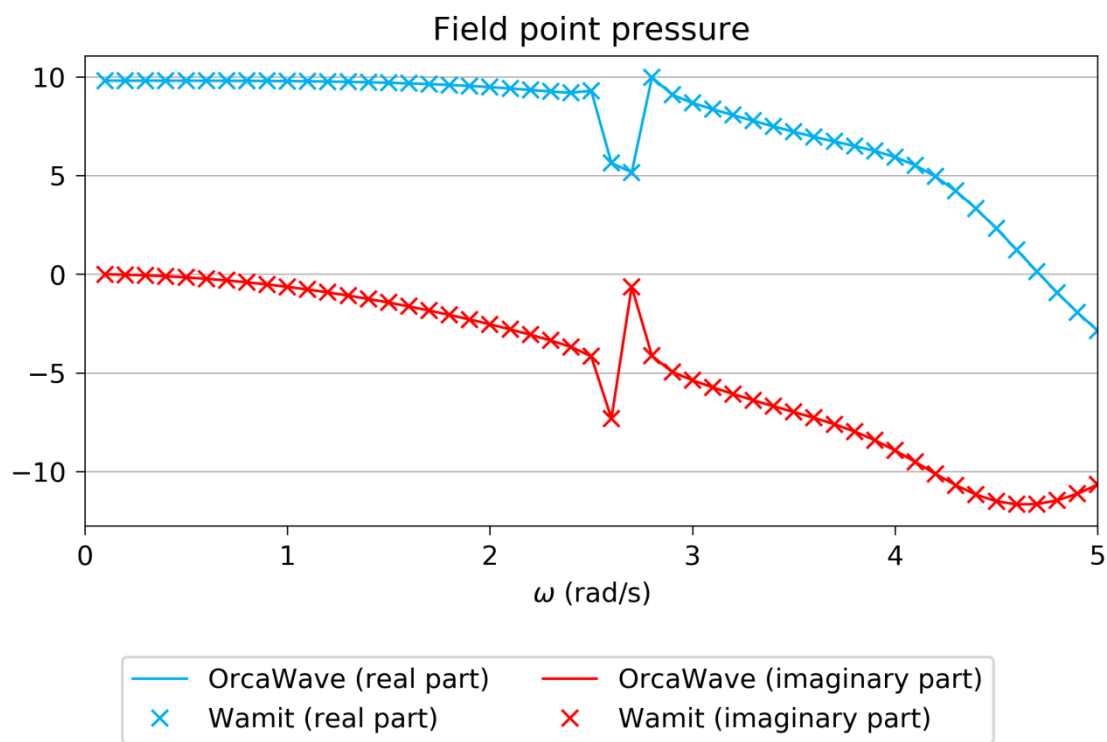


Figure 11. Sea state RAOs for $\beta = 0^\circ$: pressure at the field point (1.79, -2.1, 0) (m). The horizontal axis is angular frequency (rad/s). The vertical axis is kN/m²/m.

2.4. Floating hemisphere

2.4.1. Description

The body is a freely-floating hemisphere of radius 1m in water of infinite depth. The reason for choosing this simplistic geometry is that it is one of the very few geometries for which analytic results are available [5].

A single wave heading $\beta = 0^\circ$ and a range of wave frequencies $\omega \leq 9.90$ rad/s is considered in order to validate against the added mass and damping coefficients derived by Hulme in Tables 1-2 of [5]. The body mesh is extended to remove the effects of irregular frequencies, in this case by including panels on the interior lid in the mesh file. There are two planes of symmetry, with 814 panels representing one quadrant of the body. Figure 12 shows the mesh, with the interior free surface panels drawn in green to distinguish them from the body panels on surface of the hull.

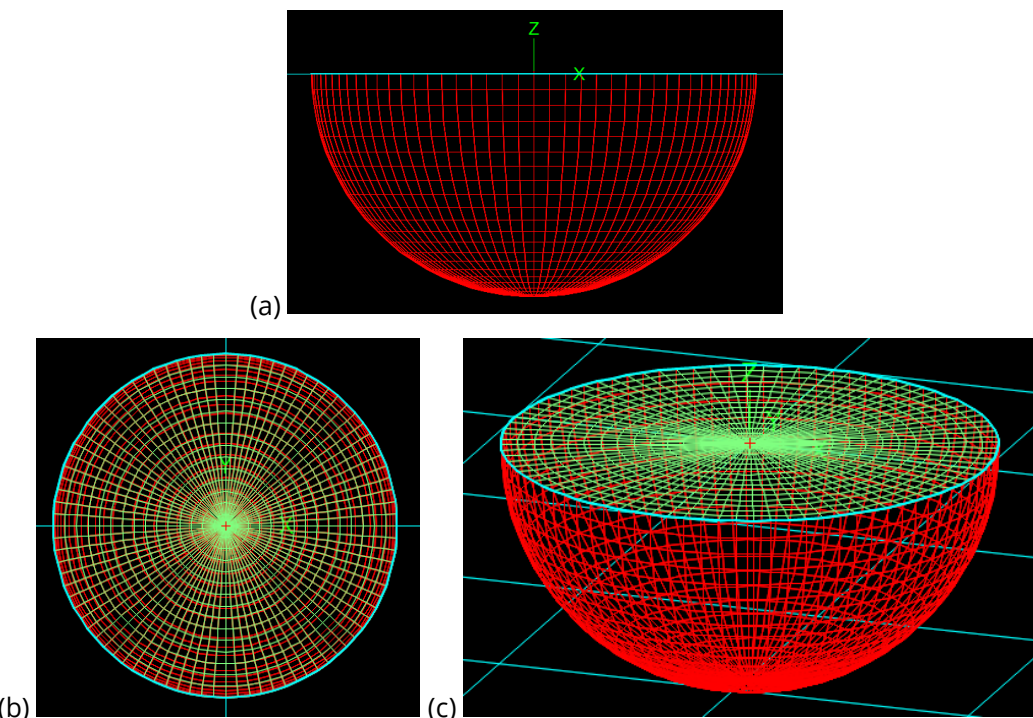


Figure 12. Elevation (a), plan (b) and perspective (c) views of the body mesh for the floating hemisphere.

2.4.2. Results

Added mass and damping coefficients are shown in Figure 13. Following our convention we plot the dimensional results reported by OrcaWave. The analytic results taken from Tables 1-2 of Hulme [5] are made dimensional by multiplying the factors given in [5].

The results in Figure 13 show excellent agreement to the analytic values, but there are of course small differences that are not visible in the figure. These differences are caused by discretisation error, i.e. the error due to solving the integral equations of potential theory using a finite mesh. The primary way to reduce discretisation errors is to refine the mesh.

2.4.3. Further considerations

For this simple geometry it is easy to construct mesh files with varying numbers of panels, so it is an ideal opportunity to demonstrate a simple convergence study using OrcaWave. In order to

make a challenging case we select the wave frequency $\omega = 6.26$ rad/s, because irregular frequency effects are seen at this frequency unless the mesh is extended over the interior free surface. Results are shown in Figure 14, confirming that the OrcaWave results for the added mass and damping coefficients do indeed converge to the analytic values as expected. We can see that the discretisation error in this case is $O(N^{-1})$, where N is the number of panels in the body mesh file.

For most body shapes analytic results are not available. Instead of the plots in Figure 14, it would be natural to plot the absolute value of, say, A_{11} against N . Alternatively the sequence of A_{11} results could be used to estimate the converged value, e.g. by taking the final value in the sequence or using a Shanks transformation, and error relative to the estimate could be plotted.

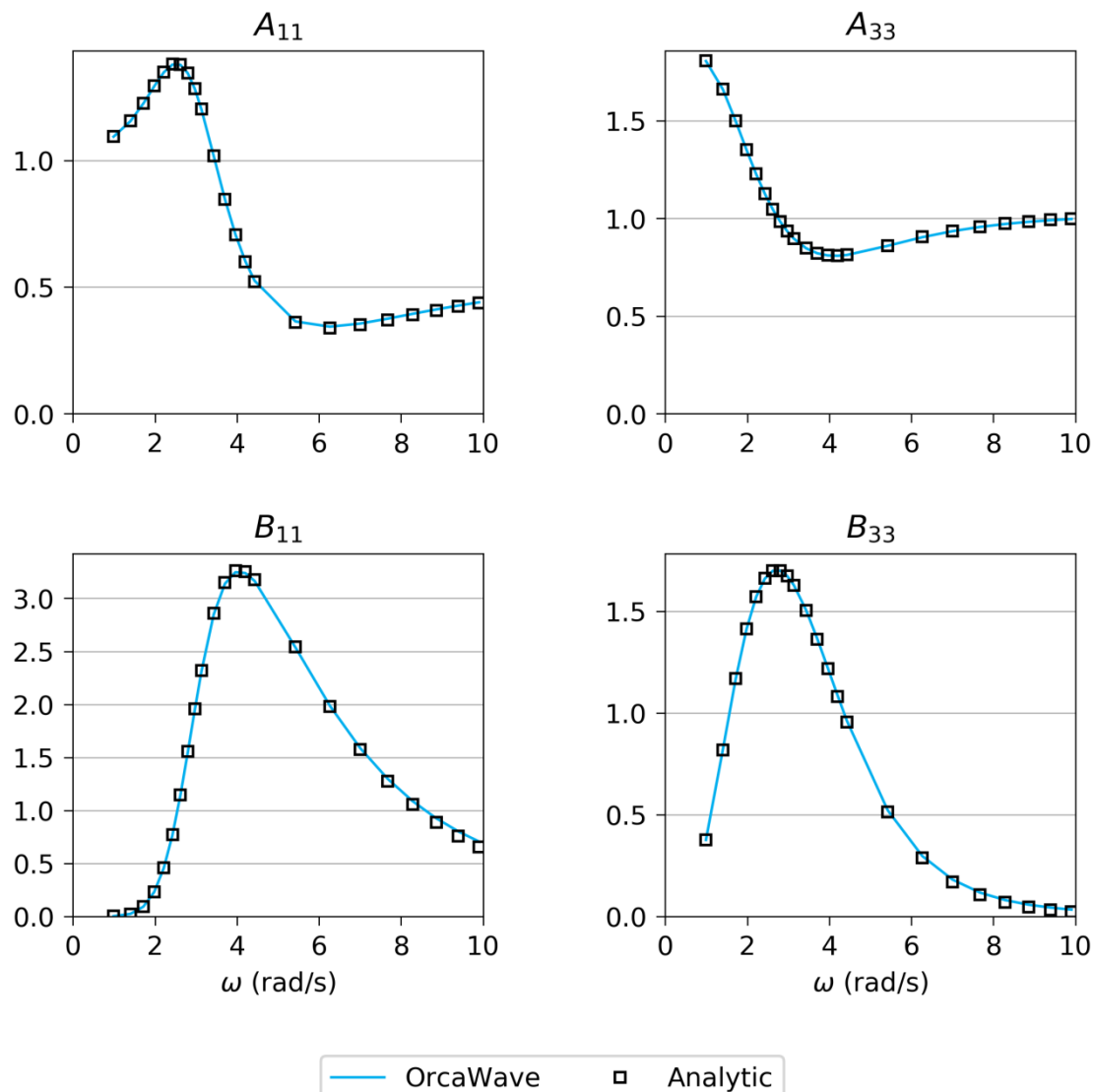


Figure 13. OrcaWave added mass (A) and damping (B) coefficients for the floating hemisphere. The horizontal axes are angular frequency (rad/s). The vertical axis is te for added mass and kN/m/s for damping.

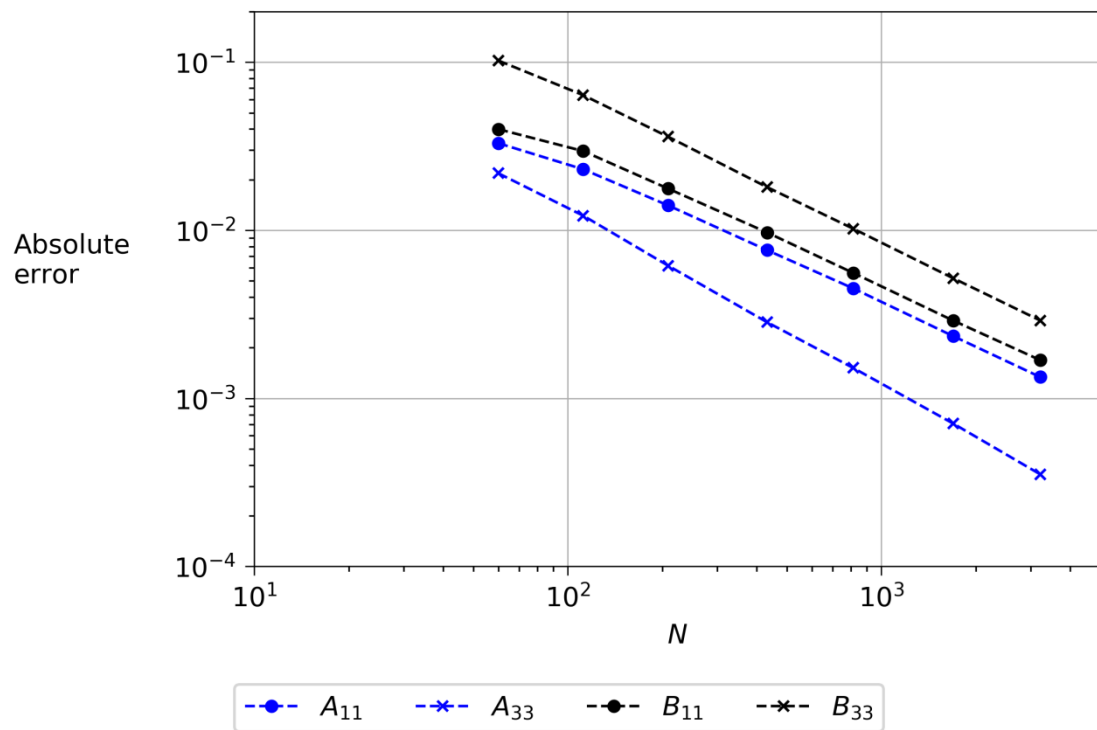


Figure 14. OrcaWave discretisation error in the added mass (A) and damping (B) coefficients for the floating hemisphere with $\omega = 6.26 \text{ rad/s}$. The horizontal axis is number of panels. The vertical axis is absolute error relative to the analytic values.

2.5. ISSC tension leg platform

2.5.1. Description

This case is based on the TEST06 and TEST06a cases of the Wamit v7.3 program. The body is the ISSC TLP [6] which has two planes of symmetry. Two body mesh files are considered, a coarse mesh with 128 panels to describe one quadrant of the body, and a fine mesh with 1012 panels to describe one quadrant. The water depth is 450m.

The heave, roll and pitch degrees of freedom are set to fixed, to model a TLP moored to the seabed with vertical cables. A single wave heading $\beta = 35^\circ$ is considered for wave periods of $10 \leq T \leq 15$ s.

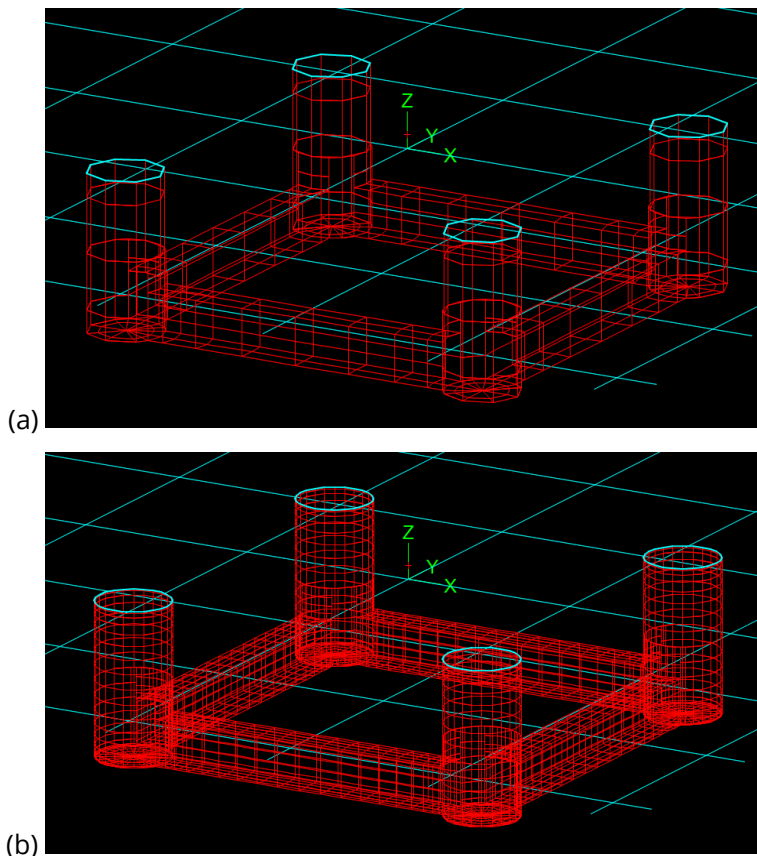


Figure 15. Perspective views of the coarse mesh (a) and fine mesh (b) of the ISSC TLP.

2.5.2. Results

The results show good agreement between OrcaWave and Wamit for both meshes. As examples, we compare the Haskind load RAOs calculated using the coarse mesh in Figure 16 and the displacement RAOs calculated using the fine mesh in Figure 17. Note that the displacement RAOs are zero in the fixed degrees of freedom: heave, roll and pitch.

We expect the discretisation error to be smaller in the fine mesh and the results to be more accurate. Since there are no analytic results in this case we do not know the true value of any of the result quantities or the precise level of discretisation error in the calculated results. However, for a given mesh there are some indicators of the discretisation error. For example, the Haskind and diffraction versions of the load RAOs are mathematically equivalent, and the difference between them in any set of results is due only to discretisation errors. The difference between

them can therefore give an indication of the discretisation error, which we demonstrate in Figure 18. In that figure we have plotted the amplitude rather than the real and imaginary parts, and we have omitted the corresponding Wamit results, purely in order to simplify the graphs. Figure 18 shows that the two forms of the load RAOs agree closely for the fine mesh (red lines) in all degrees of freedom, but that the coarse mesh (blue lines) has significant discretisation errors in the load RAOs for heave, roll and pitch.

2.5.3. Further considerations

Except for the simple cases where analytic results are known, in all other cases the best way to verify that diffraction results are sufficiently converged is to perform a convergence study using a sequence of increasingly refined meshes. It can be time consuming to prepare the meshes for a full convergence study, so indicators of discretisation error which can be inspected using results from a single mesh are very attractive. In fact there are a few such indicators:

- Symmetry of added mass and damping matrices
- Agreement of load RAOs via Haskind and diffraction methods
- Agreement of mean drift loads via pressure integration and control surface methods
- Agreement of QTF quadratic force via pressure integration and control surface methods
- Agreement of QTF potential force via direct and indirect methods

Figure 18 demonstrates how the difference between the Haskind load RAOs and diffraction load RAOs gives a useful indication of the discretisation error in the ISSC TLP case – the error is visibly much greater in the coarse mesh than the fine mesh.

However, it must be stressed that inspecting one of the metrics listed above only gives an *indication* of the discretisation errors present. For example, Figure 18 shows that performing a check of the surge load RAO, but not inspecting other degrees of freedom, would give a misleading indication of the discretisation error in the coarse mesh. Similarly, inspecting results for a single wave heading could potentially give a misleading indication. In summary, the above indicators can give some helpful reassurance, but to be certain of the level of discretisation error in a particular result quantity the best approach is to perform a convergence study.

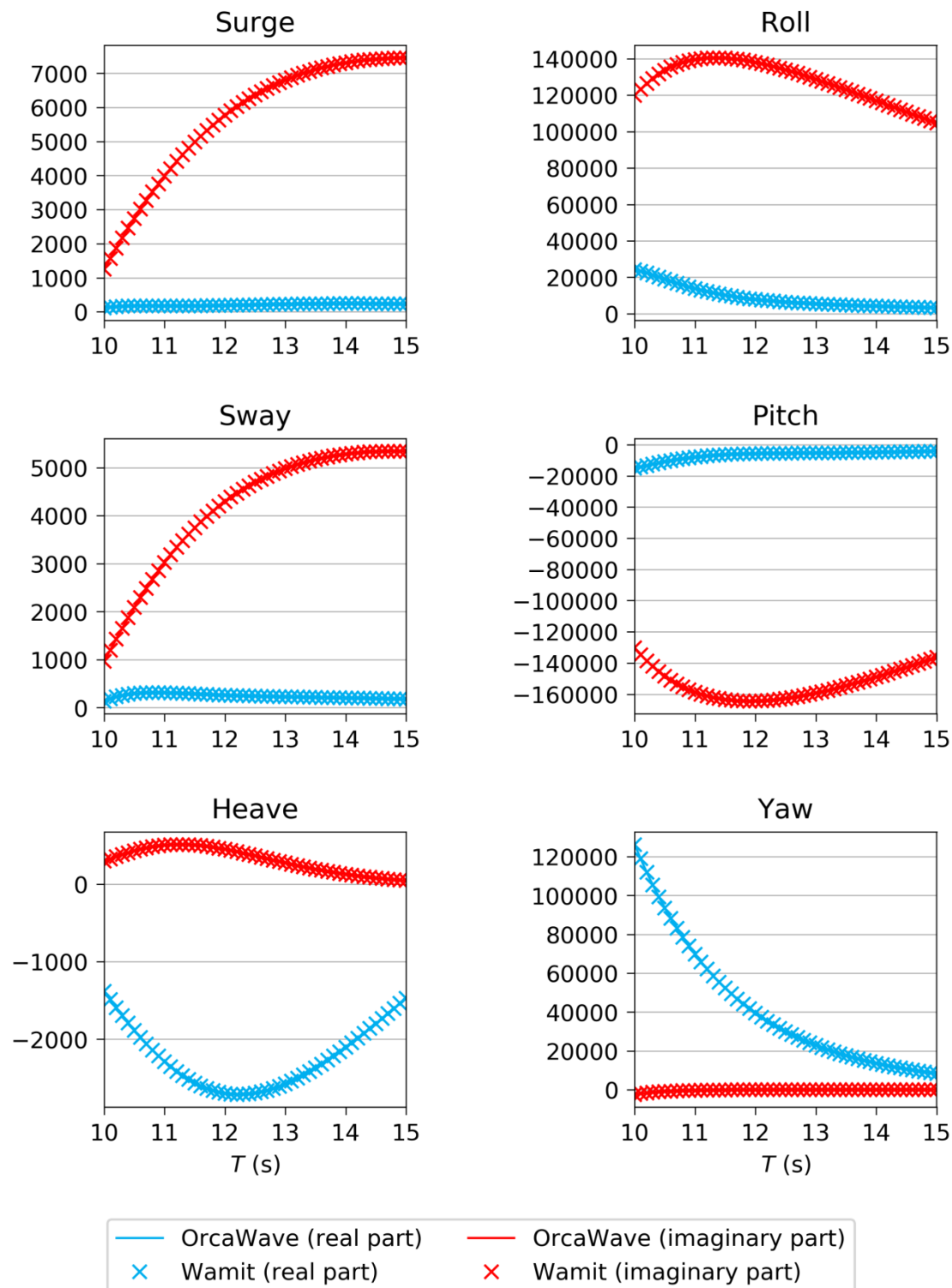


Figure 16. Haskind load RAOs for $\beta = 35^\circ$ using the coarse mesh. The horizontal axes are period (s). The vertical axis is kN/m for surge, sway and heave, kN.m/m for roll, pitch and yaw.

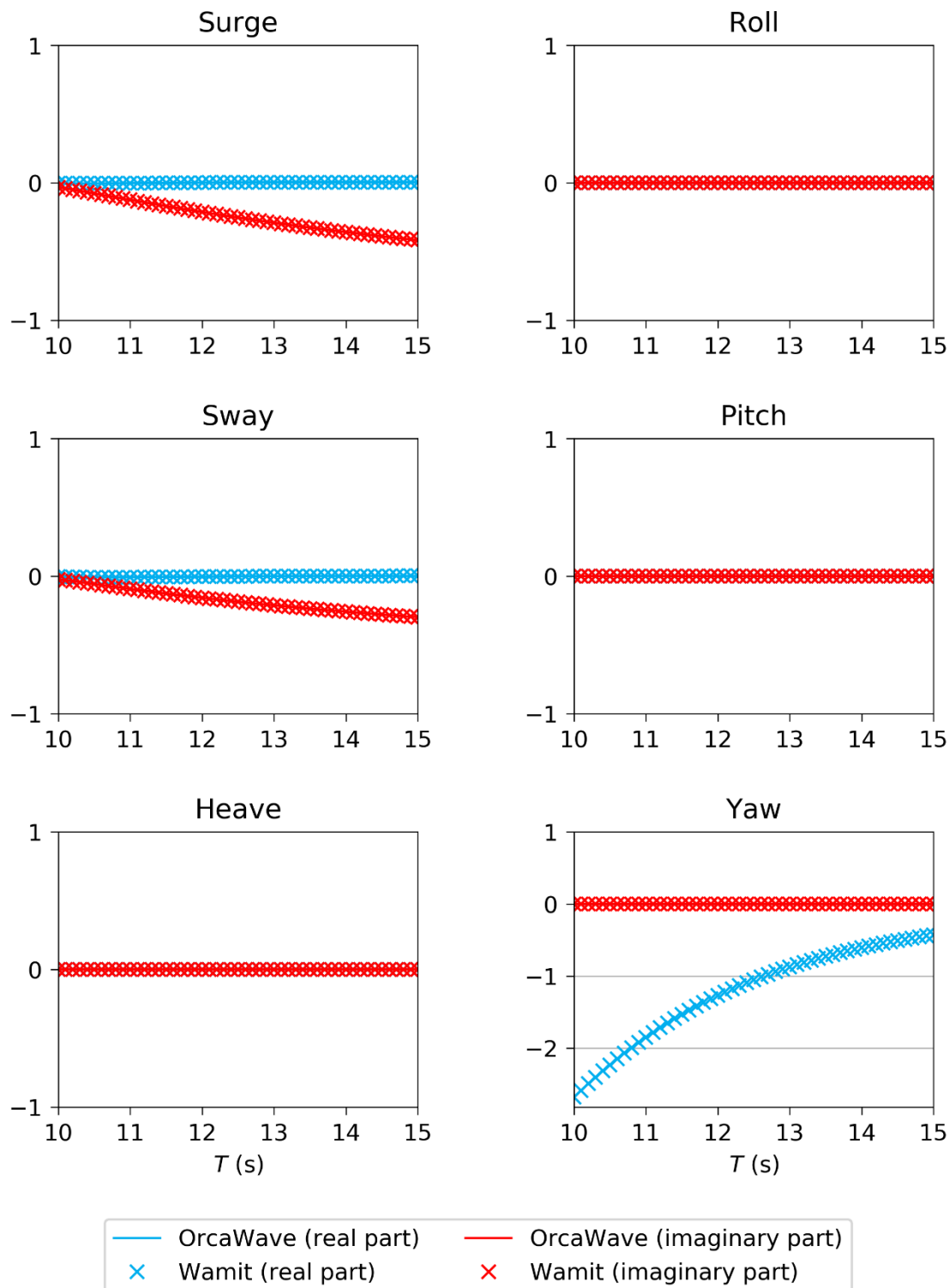


Figure 17. Displacement RAOs for $\beta = 35^\circ$ using the fine mesh. The horizontal axes are period (s). The vertical axis is m/m for surge, sway and heave, rad/m for roll, pitch and yaw.

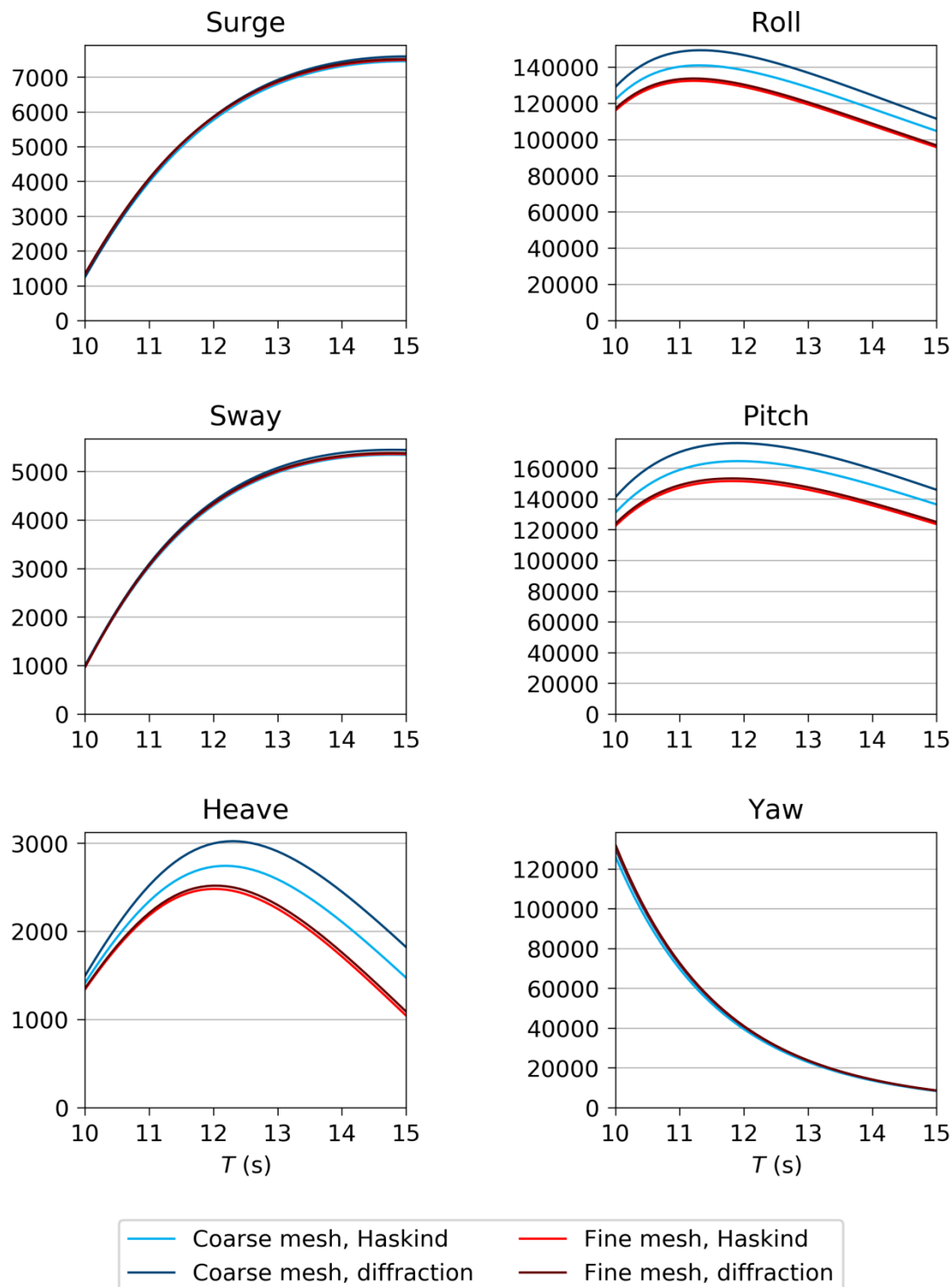


Figure 18. The amplitude of OrcaWave load RAOs for $\beta = 35^\circ$ using both the coarse and fine meshes. The horizontal axes are period (s). The vertical axis is kN/m for surge, sway and heave, kN.m/m for roll, pitch and yaw.

2.6. Multibody analysis of a circular cylinder and ellipsoid

2.6.1. Description

This case is based on the TEST05 and TEST05a cases of the Wamit v7.3 program. Two bodies are considered: a vertical cylinder and an ellipsoid. Each body has two planes of symmetry. The ellipsoid is described by 64 panels for one quadrant of the body and the cylinder by 112 panels for one quadrant of the body.

TEST05 and TEST05a have the same relative positions of the bodies and are therefore equivalent – they differ only by a 90° rotation of the entire model. In TEST05 the ellipsoid is positioned with a heading angle of 90°, meaning that the global mesh has no valid symmetry planes in OrcaWave or Wamit, whereas in TEST05a the global mesh has symmetry in the YZ plane. In the rest of this section we adopt the TEST05a configuration in order to make full use of the available symmetry.

Since the majority of the validation cases in this report consider deep water, we set the water depth to 3m in order to demonstrate an analysis in shallow water. We consider a single wave heading of 117° and a range of wave periods $1.5 \leq T \leq 3.0$ s.

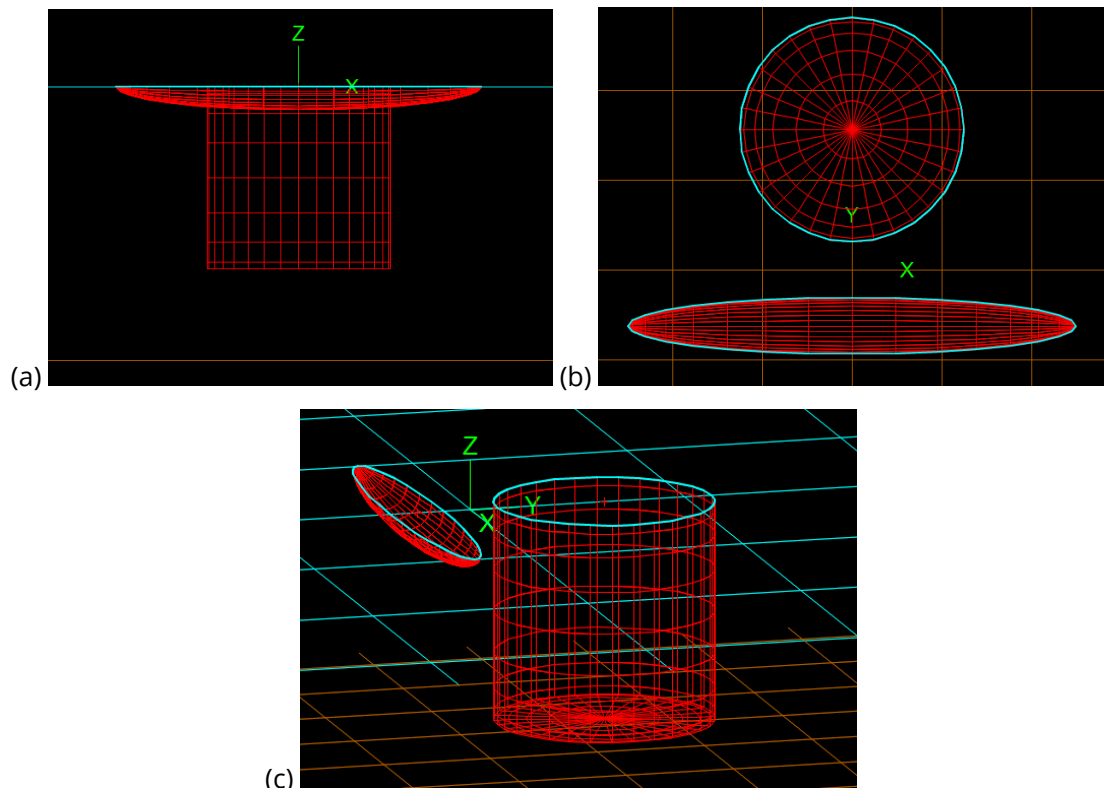


Figure 19. Elevation (a), plan (b) and perspective (c) views of the body meshes of the cylinder and ellipsoid in the TEST05a configuration.

2.6.2. Results

OrcaWave again shows excellent agreement with Wamit. For example, Figure 20 plots PI mean drift loads. The multibody system has twelve degrees of freedom in total, six per body. The degrees of freedom are independent and, strictly speaking, all twelve should be plotted separately. However, we have combined them together in Figure 20 for concision.

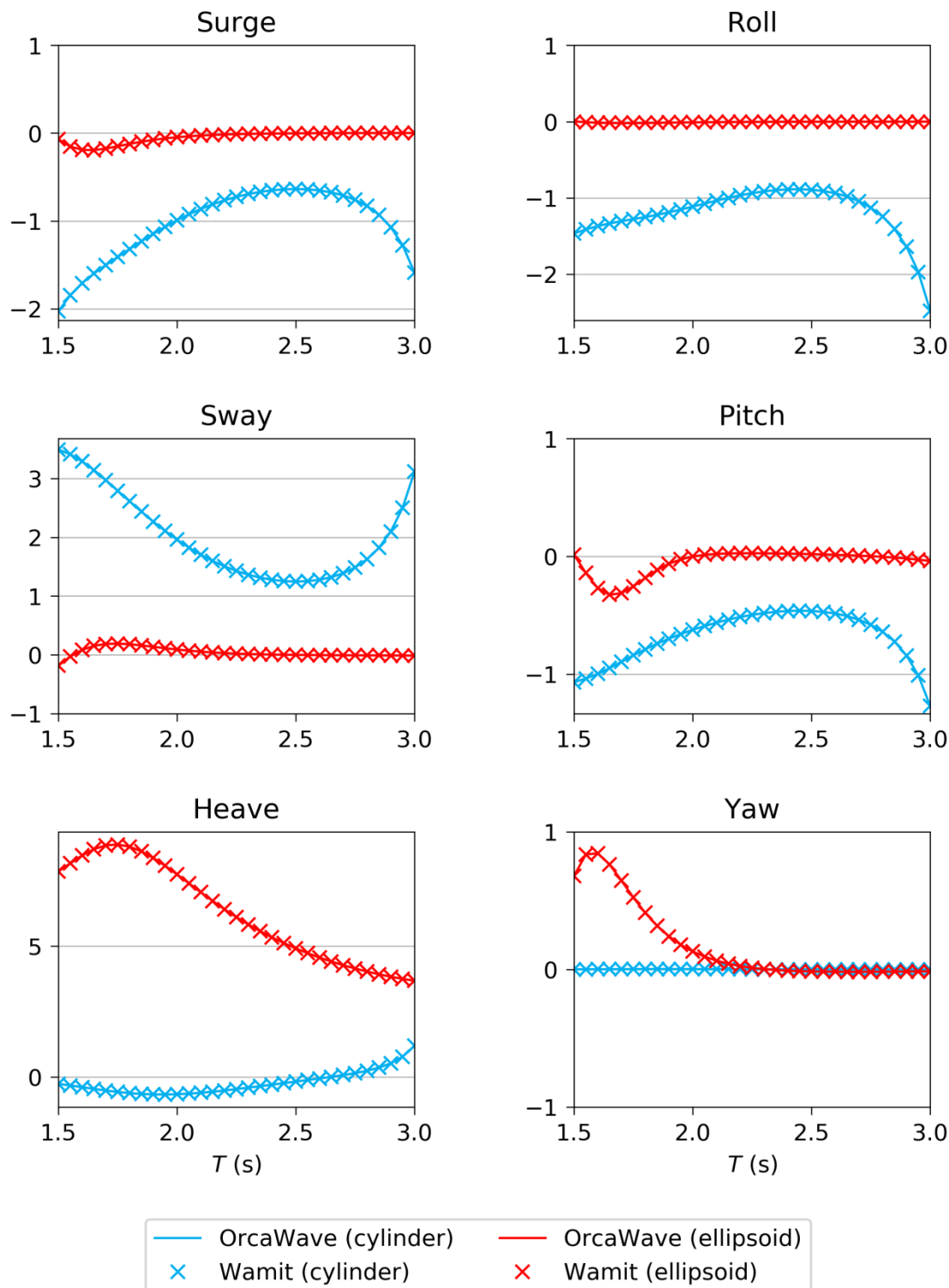


Figure 20. PI mean drift loads for $\beta = 117^\circ$. The horizontal axes are period (s). The vertical axis is kN/m² for surge, sway and heave, kN.m/m² for roll, pitch and yaw.

2.7. Inverted pyramid with control surface mean drift loads

In the preceding sections the mean drift loads presented have all been PI mean drift loads, obtained using the pressure integration method. OrcaWave can also calculate CS mean drift loads, estimates of the same loads using the control surface method. The focus of this section is to validate OrcaWave's CS mean drift load calculations.

2.7.1. Description

The body is an inverted pyramid with vertices at: (0, 0, -3), (-2, 5, 0), (8, -5, 0) and (-3, -5, 0). This shape is designed to test the mean drift load calculations in full generality: it has no symmetry planes and it intersects the free surface at an oblique angle. The reason for the latter point is that some terms in the mean drift load formulae become zero if a body intersects the free surface orthogonally – such bodies are referred to as “wall-sided”, and are avoided to make the test more comprehensive.

We use a variety of body mesh files because a convergence study will be central to our validation in this section. These are generated by a python script and have between 234 and 4704 panels to describe the body. Figure 21 shows the body mesh of 408 panels.

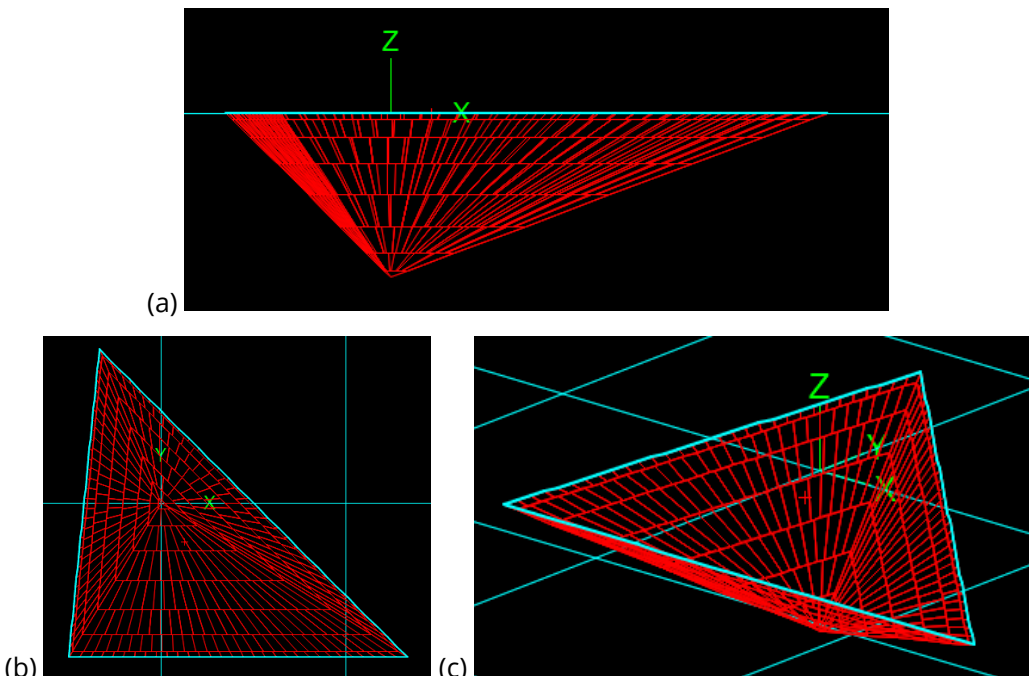


Figure 21. Elevation (a), plan (b) and perspective (c) views of the inverted pyramid body mesh with 408 panels.

In addition we also need a control surface mesh. The control surface must enclose the body, but otherwise its shape is arbitrary. We choose a pyramid shape, similar to the body and enlarged by a factor of 2. For our convergence study we will refine the control surface mesh in parallel with refinement of the body mesh, so we use a variety of mesh files having between 327 and 6963 panels. The number of panels in each control surface is approximately 1.4 times the number of panels in the corresponding body mesh. Figure 22 shows the control surface mesh of 582 panels and the body mesh of 408 panels.

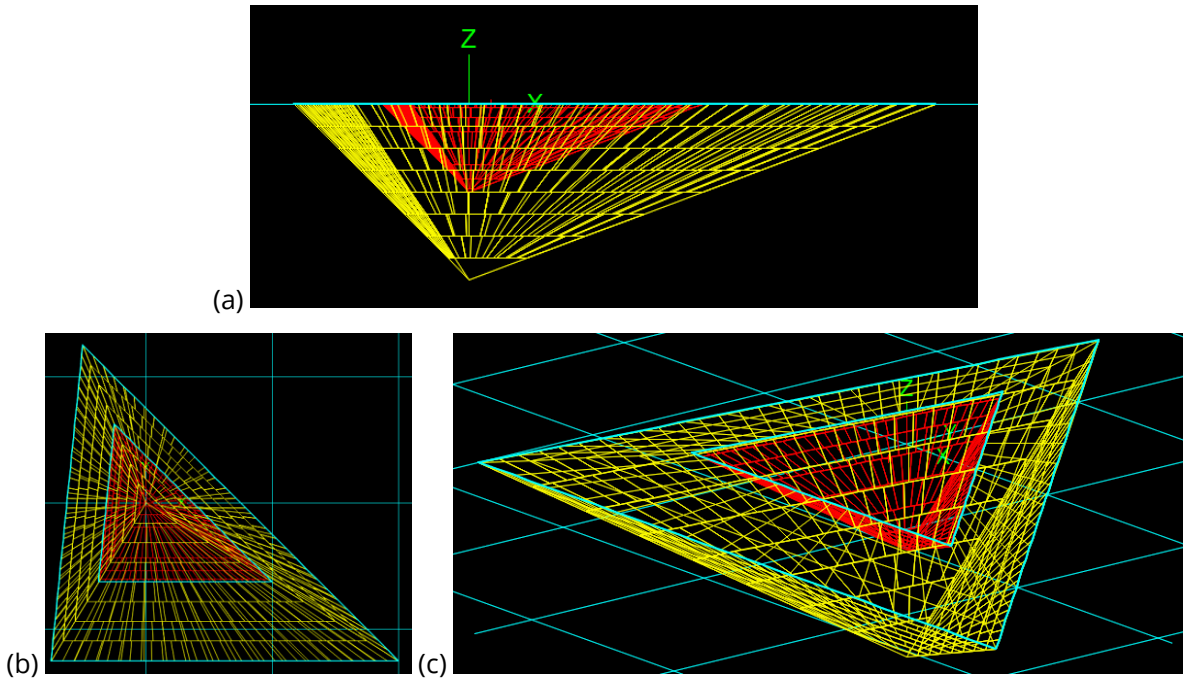


Figure 22. Elevation (a), plan (b) and perspective (c) views of the inverted pyramid body mesh (red, 408 panels) and the surrounding control surface mesh (yellow, 582 panels).

2.7.2. Results

Initially we use the mesh files shown in Figure 22, a range of wave headings $\beta = 0^\circ, 20^\circ, 40^\circ, \dots, 340^\circ$ and a range of wave periods $4 \leq T \leq 8$ s. The wave periods are chosen to avoid irregular frequencies, which are expected for $T \lesssim 2.8$ s, in order to keep the analysis as simple as possible. The mean drift loads by both methods are shown in Figure 23 for the wave heading $\beta = 0^\circ$. The PI loads show good agreement between OrcaWave and Wamit, similar to the results in earlier sections of this report. For CS loads, good agreement is seen between OrcaWave and Wamit for surge, sway and yaw, but there are significant differences for heave, roll and pitch. Although we initially suspected a bug in our OrcaWave code, after further investigation we believe that the error is in the Wamit calculation. We explain our reasoning below.

The two different methods to calculate mean drift loads give us another way to test the validity of the results. As discussed in Section 2.5.3, the two methods are mathematically equivalent and the difference between them is due only to discretisation errors. We note that in Figure 23 the PI loads, for which the two programs agree, are generally closer to OrcaWave's CS loads than to Wamit's CS loads – this is suggestive but not conclusive. To proceed further we perform a convergence study and test whether the CS and PI loads converge to the same limit when the number of panels $N \rightarrow \infty$, as theory predicts they must.

We select $T = 5$ s for the convergence study, a representative wave period in Figure 23. We refine both the body mesh and the control surface mesh in parallel, as described above. Figure 24 shows results for the maximum absolute difference between the dimensional CS and PI loads, taking the maximum over all pairs of wave headings with $\beta = 0^\circ, 20^\circ, 40^\circ, \dots, 340^\circ$. For OrcaWave we see that the difference tends to zero in each degree of freedom as $N \rightarrow \infty$. For Wamit we do not see the difference tending to zero in the heave, roll and pitch degrees of freedom. We therefore conclude that the convergence study validates the OrcaWave results for CS loads, and shows that the Wamit results are erroneous.

2.7.3. Further considerations

The shape of the pyramid body used in this section is intended to be generic, but there is a risk that it may be a special case for some reason we don't know. To check that possibility, we perform a similar analysis in Section 2.8 to validate CS mean drift loads for an ellipsoidal body.

Our choice of convergence metric in Figure 24 is significant. We believe that taking the maximum over all heading pairs, combined with treating each degree of freedom individually, is a robust convergence test. In contrast, taking a single wave heading and degree of freedom in isolation can give a misleading indication of convergence in some circumstances. For example, Chen [8] demonstrates this by plotting the surge and sway mean drift forces for an FPSO at a single oblique wave heading. In that particular case the surge force gives no indication of the true level of the discretisation error in the PI mean drift force. For our purposes, studying a single heading could give an unrepresentative indication of the level of convergence, whereas the maximum error over all headings is a better metric.

We are not aware of any theoretical predictions for the convergence rates of diffraction results that apply to general body shapes. However, it is well known that PI mean drift loads often converge more slowly with respect to mesh refinement than RAOs, added mass and damping. CS mean drift loads are said [7] to converge faster than PI loads for surge, sway and yaw. Whether the same is true of heave, roll and pitch is unclear.

Given the possibility of slow convergence, large discretisation errors may be present in mean drift loads even if the RAOs, added mass and damping are all satisfactorily converged. When performing an analysis it is therefore especially important to test the accuracy of mean drift load results. Ideally a convergence study would be performed, or failing that a check on the consistency of CS and PI loads can give an indication of discretisation error. In either case it is advisable to include all relevant wave headings and degrees of freedom in the test of accuracy.

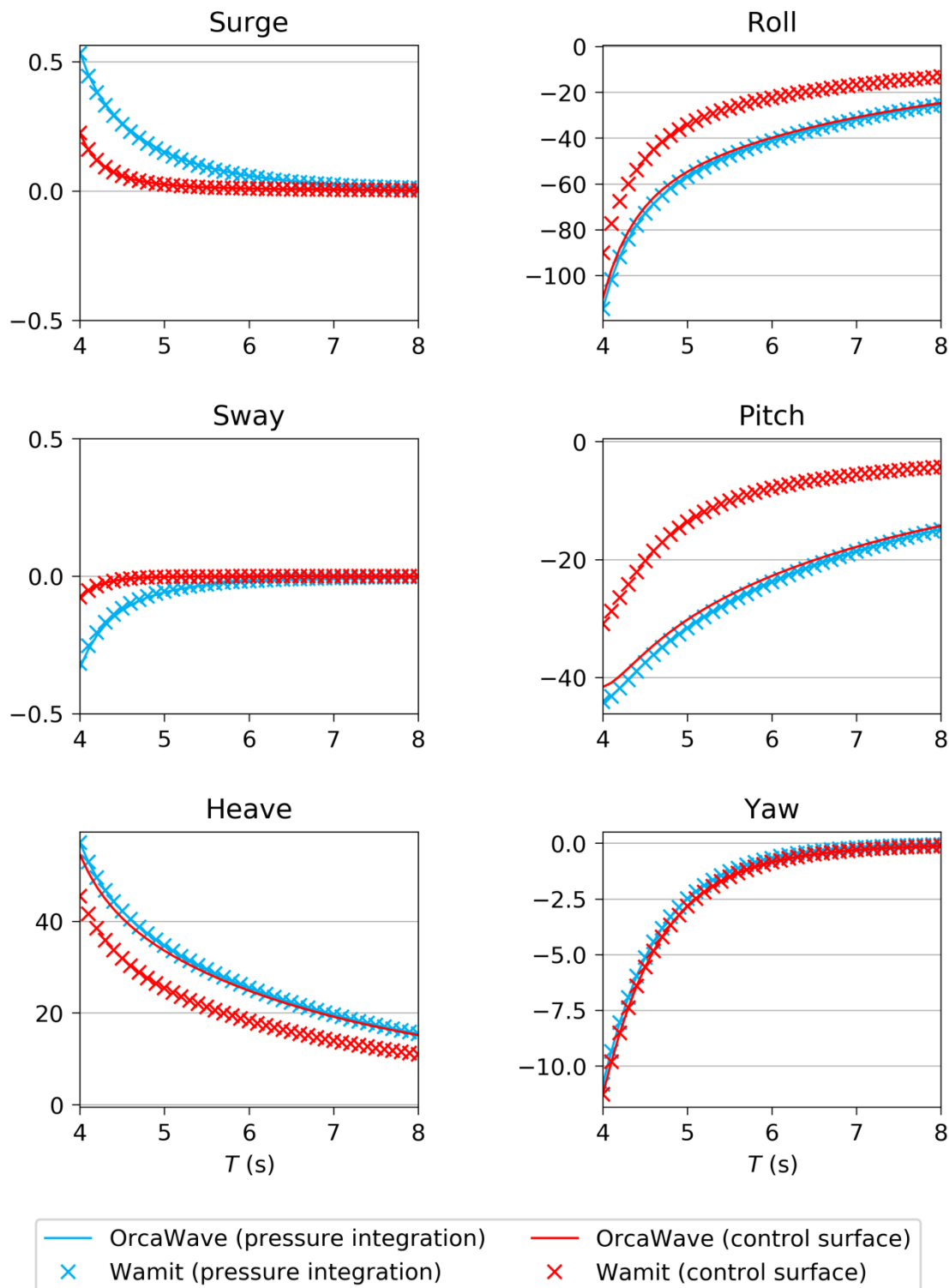


Figure 23. CS and PI mean drift loads for $\beta = 0^\circ$ using the meshes shown in Figure 22. The horizontal axes are period (s). The vertical axis is kN/m^2 for surge, sway and heave, kN.m/m^2 for roll, pitch and yaw.

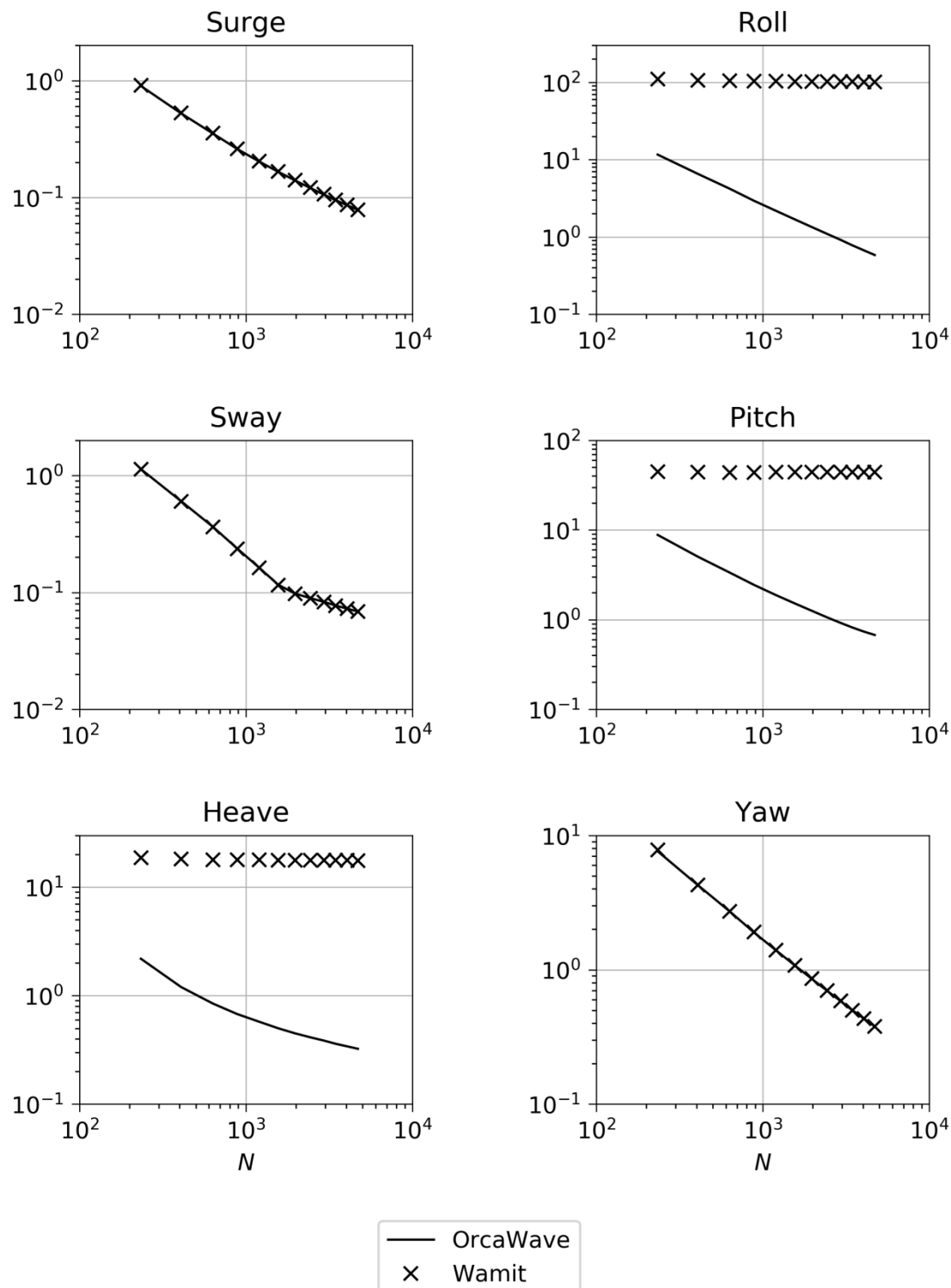


Figure 24. Mean drift load convergence study results for wave period $T = 5$ s. The horizontal axis is number of panels in the body mesh; each control surface mesh has approximately 1.4 times as many panels. The vertical axes are maximum absolute difference, over all heading pairs, between CS and PI loads.

2.8. Ellipsoid with control surface mean drift load

2.8.1. Description

The aim of this section is to perform a validation of CS mean drift load calculations similar to Section 2.7, but using a different body. The body is an ellipsoid given by

$$\frac{1}{2}x^2 + y^2 + (z - z_0)^2 = 1$$

where (x, y, z) are in metres and $z_0 = 0.2\text{m}$. We use a nonzero value of z_0 to ensure that the body is not wall-sided, for the same reason as in the previous section. We use a single representative wave period $T = 2\text{s}$ for the convergence study and the same range of wave headings as above: $\beta = 0^\circ, 20^\circ, 40^\circ, \dots, 340^\circ$.

The body has two planes of symmetry. The control surface is taken to be the same shape as the body, enlarged by a factor of 2, and also has two planes of symmetry. Figure 25 shows the body and control surface, using 96 panels to describe one quadrant of each.

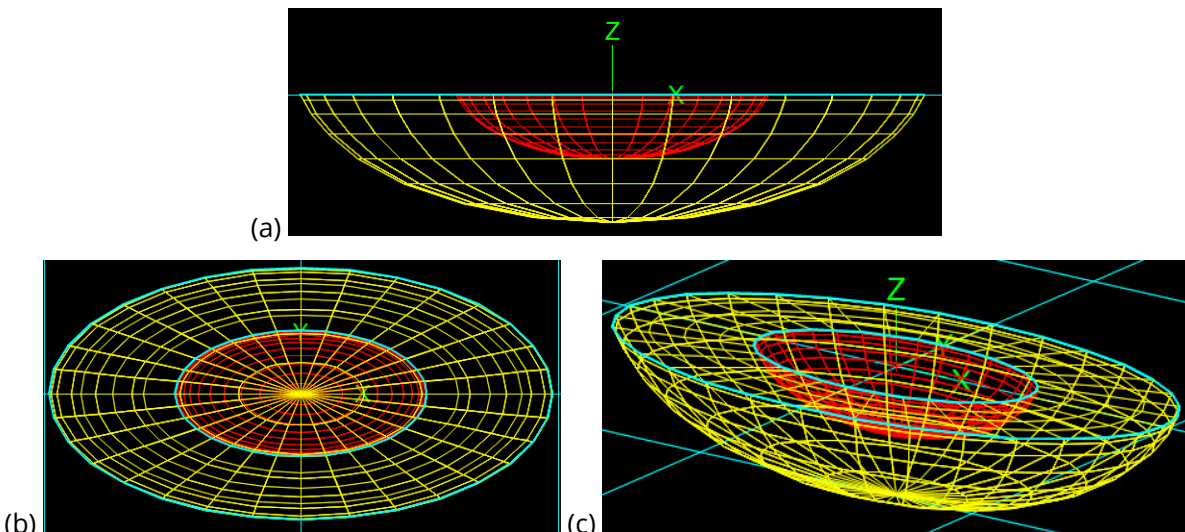


Figure 25. Elevation (a), plan (b) and perspective (c) views of the ellipsoid body mesh (red) and the surrounding control surface mesh (yellow). Both meshes have 96 panels per quadrant.

2.8.2. Results

The convergence study results are shown in Figure 26. They follow the same pattern as Figure 24 for the pyramid body. For OrcaWave we see that the difference tends to zero in each degree of freedom as $N \rightarrow \infty$. For Wamit we do not see the difference tending to zero in the heave, roll and pitch degrees of freedom. We conclude that this case adds further validation to the OrcaWave results for CS loads, and shows that the Wamit results are erroneous.

2.8.3. Further considerations

In this section and in Section 2.7 we have drawn particular attention to the fact that the bodies are not wall-sided. We believe it is relevant because we have investigated a handful of wall-sided bodies and obtained good agreement between CS load results from OrcaWave and Wamit. For example, we have found good agreement for a hemisphere (see Section 3.2) and for various vertical cylinders and prisms.

To give a concrete example, we can modify the geometry of the ellipsoid considered above. Changing the value of z_0 to zero makes the ellipsoid wall-sided. After making this change we re-run the same analysis and generate the results shown in Figure 27. Figure 27 shows that the CS and PI loads are tending to a common limit as $N \rightarrow \infty$ in both programs. Hence, for this wall-sided body, both OrcaWave and Wamit pass this convergence test.

Based on a handful of test cases, our tentative hypothesis is that the Wamit CS load results are correct for wall-sided bodies, but are in error for bodies that are not wall-sided. We communicated this hypothesis and our relevant mesh files to Wamit Inc. in September 2019. We are in a continuing dialogue with Wamit Inc. about these results.

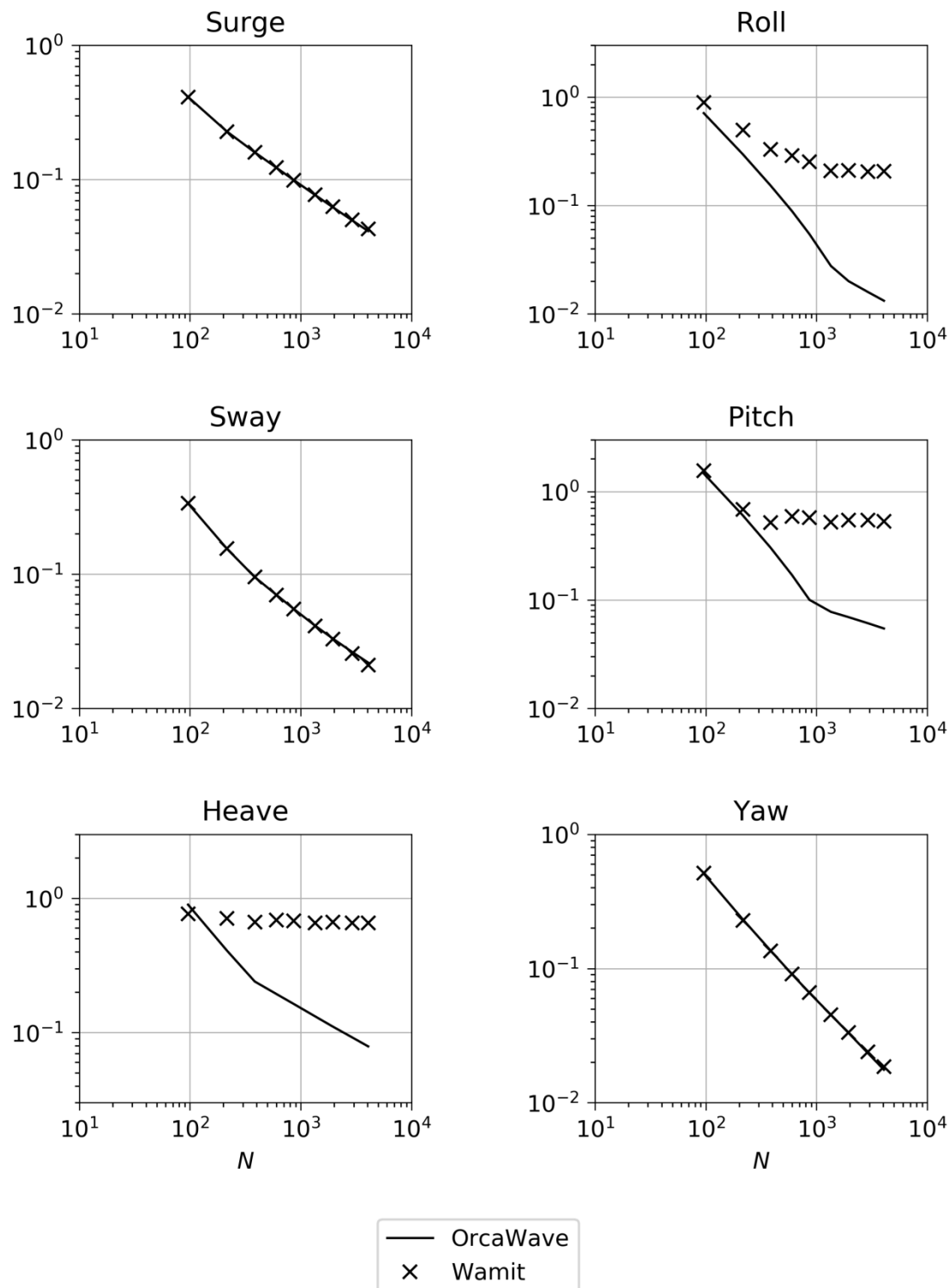


Figure 26. Mean drift load convergence study results for wave period $T = 2$ s. The horizontal axis is number of panels per quadrant for both body mesh and control surface mesh. The vertical axes are maximum absolute difference, over all heading pairs, between CS and PI loads.

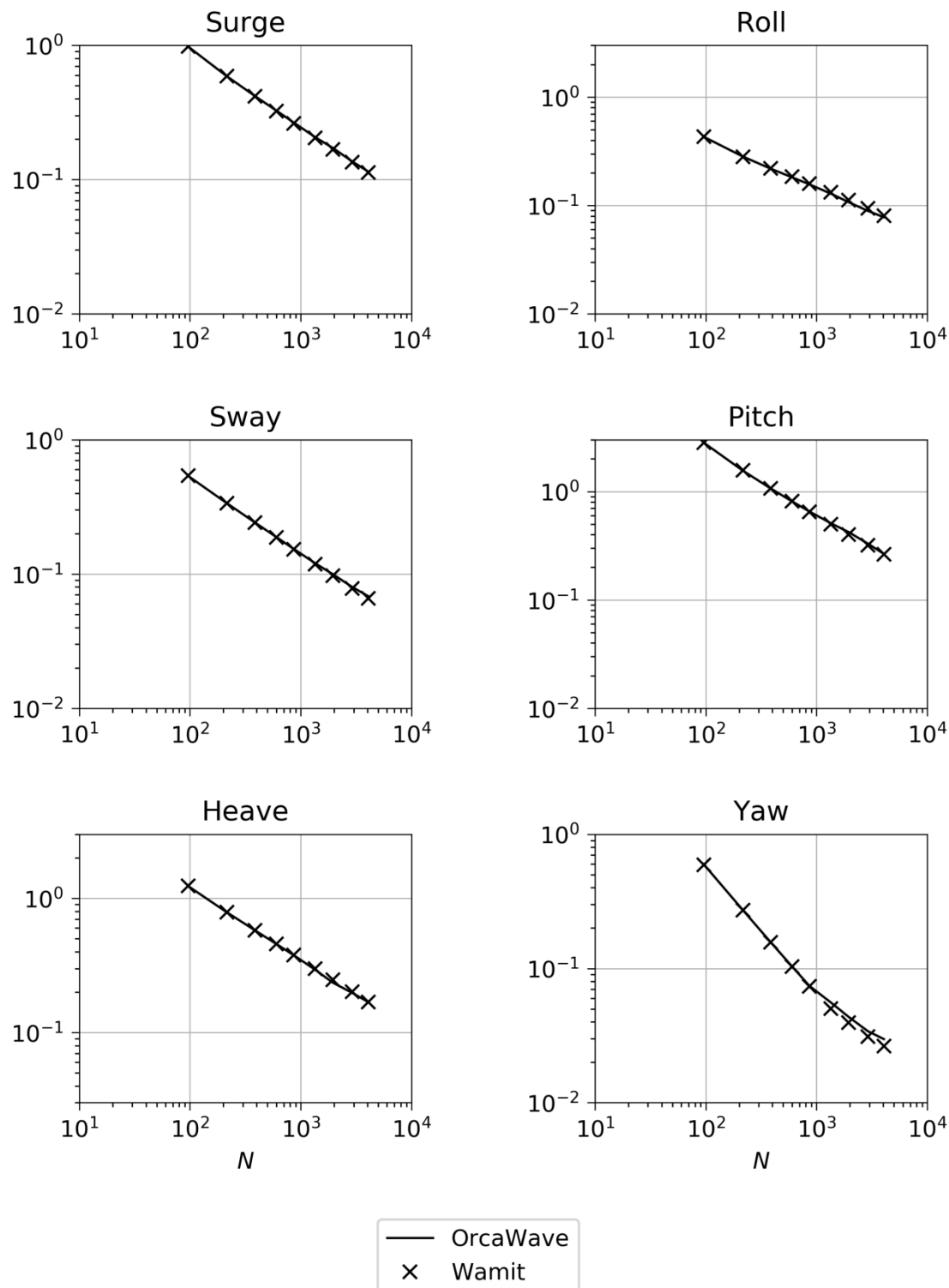


Figure 27. Mean drift load convergence study results for a wall-sided ellipsoid ($z_0 = 0$) with wave period $T = 2$ s. The horizontal axis is number of panels per quadrant for both body mesh and control surface mesh. The vertical axes are maximum absolute difference, over all heading pairs, between CS and PI loads.

2.9. Circular cylinder with moonpool and damping lid

2.9.1. Description

This case is based on the TEST02 case of the Wamit v7.3 program. The body is a vertical cylinder of radius 0.5m and draught 1m, with a cylindrical moonpool of radius 0.25m at its centre. The water depth is infinite. The body mesh has two planes of symmetry, with 368 panels to describe one quadrant of the body.

Moonpools introduce hydrodynamic resonances associated with pumping or sloshing motion of the water in the moonpool at particular frequencies. For this body the first resonant frequency is at $\omega \approx 2.9$ rad/s. In pure potential theory (with no additional damping applied) its effect is seen as large-amplitude responses in the heave components of added mass, damping, load RAOs and displacement RAOs.

A damping lid is placed on the surface of the moonpool to provide numerical damping of these non-physical responses. The damping lid is represented by 32 panels to describe one quadrant.

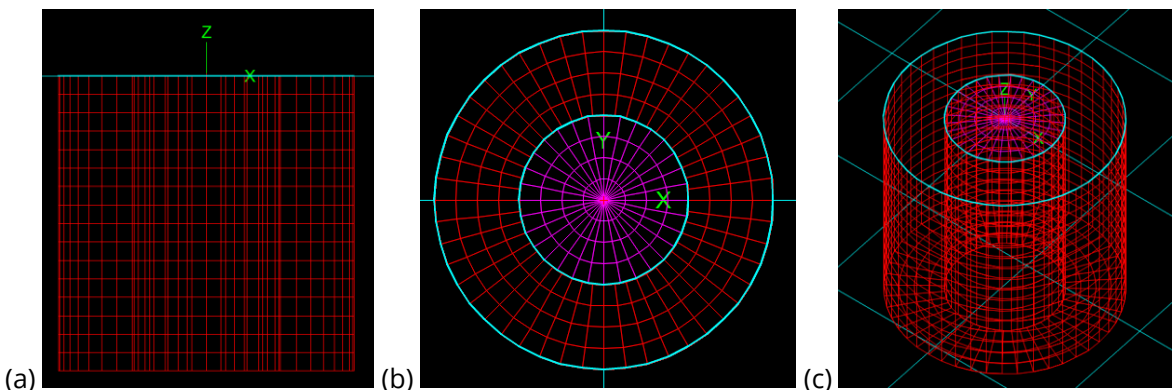


Figure 28. Elevation (a), plan (b) and perspective (c) views of the body mesh (red) and the damping lid mesh (purple).

2.9.2. Results

A selection of results corresponding to the heave degree of freedom, i.e. the components which display resonant behaviour, is plotted in Figure 29. For simplicity we plot the magnitude, rather than the real and imaginary parts, of the RAOs.

Figure 29 shows excellent agreement between OrcaWave and Wamit for the case with no damping lid. Resonant behaviour is seen as a singularity at the resonant frequency $\omega \approx 2.9$ rad/s for the added mass, damping and load RAO. The displacement RAO is a more complicated picture, having a large (but finite) peak at $\omega \approx 2.75$ rad/s and an apparently singular peak at $\omega \approx 3.00$ rad/s.

Figure 29 also includes OrcaWave runs with the damping lid present using two different values of the damping factor ϵ . In general, small values of ϵ are appropriate in order to ensure that the impact of the damping lid is negligible at frequencies away from the resonance. We see that OrcaWave's damping lid has the desired effect in Figure 29: the singularities are removed, but away from the resonant frequency the results are unaffected.

We note that Figure 29 shows the same qualitative damping effect on the displacement RAO as shown in Figure A.1 of [2]. However, when a damping lid is present direct comparison between

OrcaWave and Wamit is difficult because OrcaWave and Wamit use different damping models. This is discussed in more detail below.

2.9.3. Further considerations

We noted above that the damping lid models in OrcaWave and Wamit differ. Specifically, OrcaWave [1] uses the same model as HydroStar [7], in which the velocity potential satisfies the following boundary condition on the damping lid

$$g \frac{\partial \phi}{\partial z} - \omega^2 [1 - i\epsilon] \phi = 0$$

Of the various options available in Wamit the closest is `IDAMPER=1`, for which the velocity potential satisfies the following boundary condition on the damping lid (see eq. 15.92 of [2])

$$[g + i\omega e] \frac{\partial \phi}{\partial z} - \omega^2 \phi = 0$$

We use different symbols to emphasise that Wamit's damping parameter e is not the same as OrcaWave's damping factor ϵ . Note that e has the dimensions of a velocity, whereas ϵ is dimensionless.

The two models are formally equivalent if we equate

$$e = \frac{g\epsilon}{\omega} (1 - i\epsilon)^{-1}$$

Since both ϵ and e are entered into the programs as real numbers we cannot choose values that are exactly equivalent. However, if $\epsilon \ll 1$ then we can approximate $e \approx g\epsilon/\omega$. This is our best opportunity to create models in the two programs that are comparable.

Figure 29 includes a Wamit run with $e = 0.054$ m/s, to approximate $\epsilon = 0.016$ at the resonant frequency. The results closely match the corresponding OrcaWave case as expected, validating the OrcaWave results. Note however that for larger ϵ , or over a broader frequency range, this approximation will not necessarily give such closely equivalent models in the two programs.

It is important to remember that the damping lid models above, and the large family of similar alternatives, are empirical: they are effective at damping resonant responses, but they do not directly model the physics that is neglected by potential theory. It is always necessary to choose the damping factor ϵ with care, and to verify that it achieves a desired damping effect on the model in question.

Finally, we note that the hydrodynamic resonances discussed in this section are in a different category to body motion resonances (e.g. roll or heave resonance). Hydrodynamic resonances are usually associated with confined regions of water, such as a moonpool or a small gap between two large vessels. Without a damping lid, they cause unrealistically large responses in added mass, damping or load RAO results (see Figure 29). In contrast, body motion resonances are seen as spikes in displacement RAOs, but without any corresponding spikes in the added mass, damping or load RAOs (see Section 2.1.2).

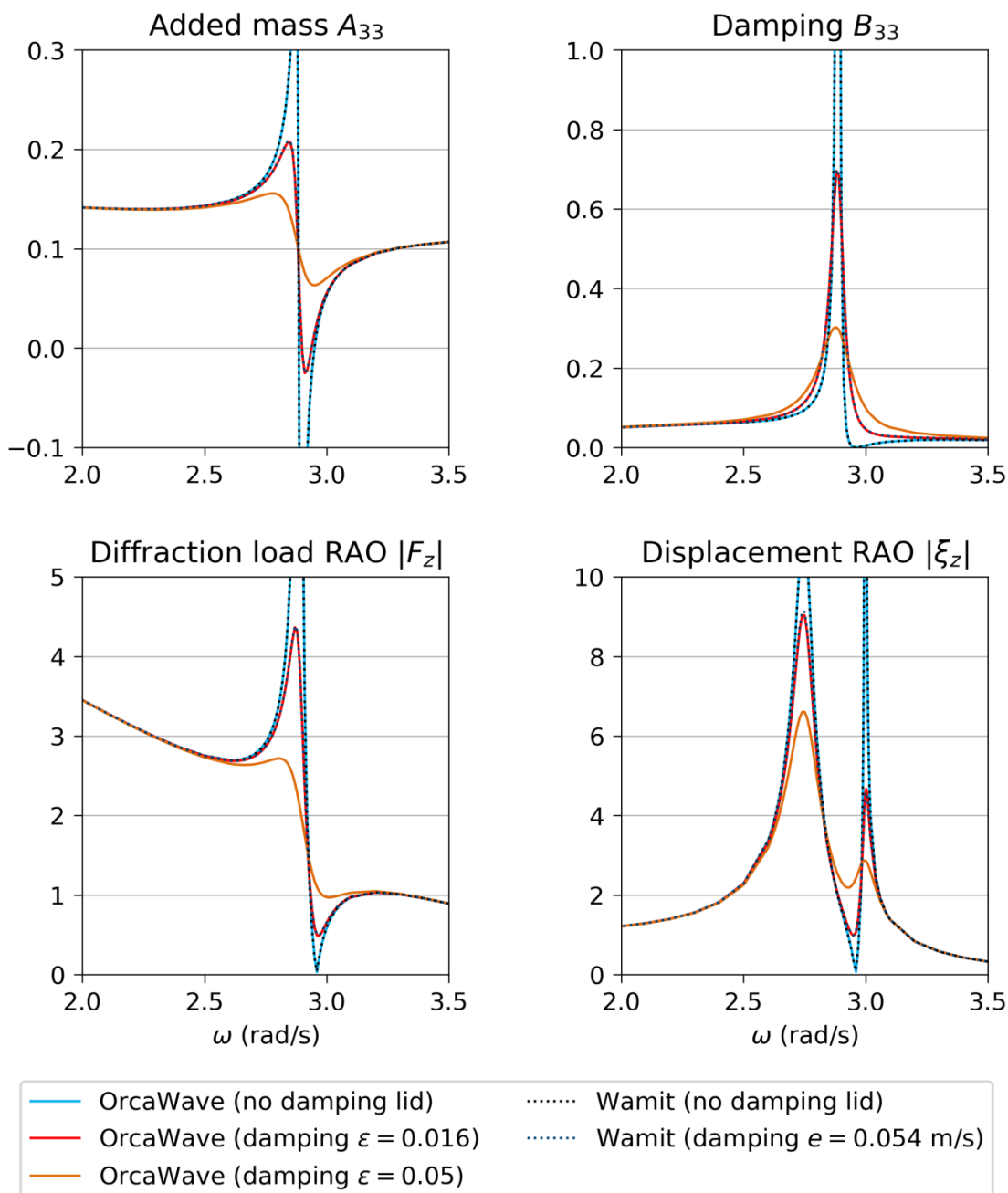


Figure 29. Heave components of added mass, damping, load RAO and displacement RAO for the cylinder with moonpool. The horizontal axes are angular frequency (rad/s). The vertical axes are te, kN/m/s, kN/m and m/m respectively.

3. Second-order validation cases

3.1. QTFs of a bottom-mounted circular cylinder

3.1.1. Description

The body is a vertical circular cylinder, fixed in position and extending from the seabed to the free surface. This geometry makes an ideal validation case because analytic results are available for the QTFs [9], and it is also the basis of the TEST102 case of the Wamit v6.4S program.

Following TEST102 of Wamit v6.4S, the water depth is 1m and the radius of the cylinder is 1m. The body has two planes of symmetry and is described by a gdf file with 100 panels per quadrant. We consider a range of wave frequencies $0.5 \leq \omega \leq 3.0$ rad/s. The first irregular frequency is estimated at 4.7rad/s for this body. The sum frequencies of the second-order analysis extend up to 6.0 rad/s and therefore it is advisable to extend the mesh to remove irregular frequency effects. The extended mesh has 170 panels per quadrant.

To calculate QTFs we also need a panel mesh of the free surface panelled zone. This extends to a radius of 3m and is described by an fdf file with 252 panels per quadrant. There is no quadrature zone, and the asymptotic zone is therefore defined by radii greater than 3m.

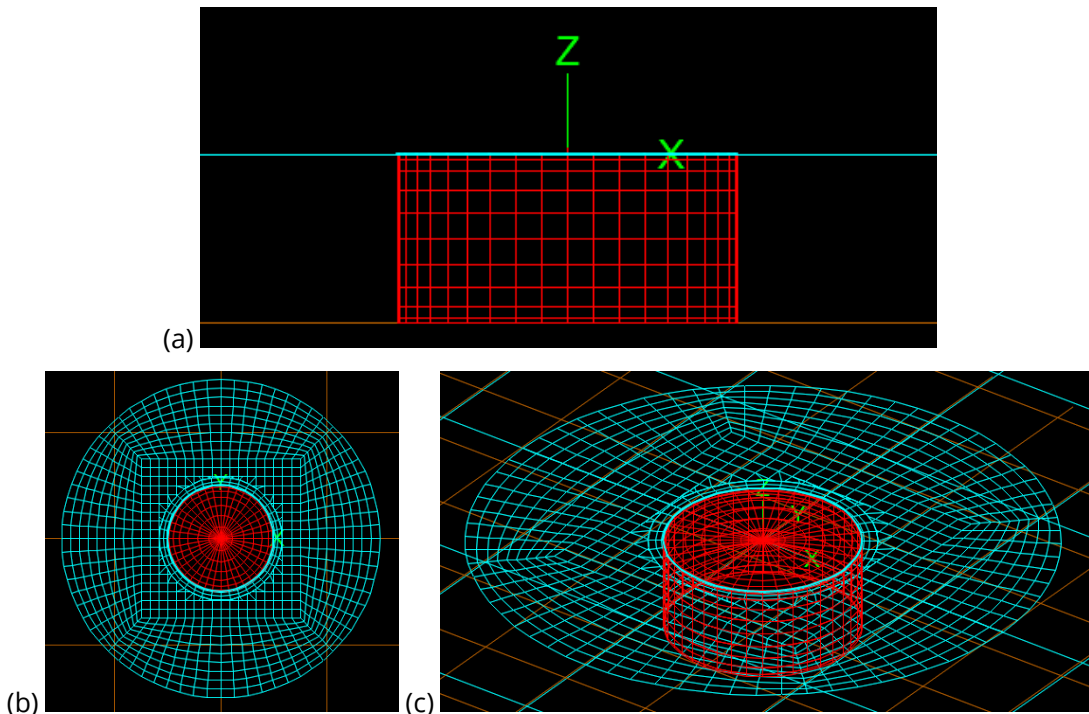


Figure 30. Elevation (a), plan (b) and perspective (c) views of the body mesh (red) and the free surface panelled zone mesh (blue).

3.1.2. Results

The analytic results in [9] pertain to monochromatic and unidirectional waves, specifically the surge component of sum-frequency QTFs. This guides our choice of wave frequencies and headings to analyse in OrcaWave and Wamit for this case. Results for surge force are shown in Figure 31. We see excellent agreement between the two programs as well as with the analytic values computed from the formulae in [9].

Load RAO and PI mean drift load are included in Figure 31 because, although we have already validated them in the earlier sections of this report, it is unusual to have analytic values for comparison. We see that the discretisation error for this mesh (i.e. the difference between computed and analytic values) is negligible for the load RAO. PI mean drift loads are known to converge slowly with respect to mesh size, so it is not surprising that small discretisation error is visible in this quantity, particularly for the shortest waves.

The quadratic and potential load components of the full QTF also show excellent agreement. In this case these are the loads at frequency 2ω due to an incident wave of frequency ω . The quadratic load is computed in an analogous fashion to mean drift load, and it too can be computed by either PI or CS methods. For simplicity we only present PI quadratic loads here, refer to Sections 2.7, 2.8 and 3.2 for discussion of CS loads.

The sum-frequency potential load is the load due to the second-order velocity potential. The direct and indirect methods are two mathematically equivalent ways to compute the same force, loosely analogous to the diffraction and Haskind methods, respectively, for load RAOs. We show both methods here for the purpose of validation, but note that there is additional cost to compute the indirect method in OrcaWave (unlike the two load RAO methods, where the cost of computing both is negligible). Therefore, in a real analysis, it may be best to compare the two methods for a subset of cases to get an indication of discretisation error, but to choose one method for the production run.

3.1.3. Further considerations

We have only presented QTF results in this section for the special case of sum-frequency QTFs due to monochromatic and unidirectional waves, in order to allow comparison with the available analytic results. The fact that the body is fixed also makes the calculation something of a special case – the algebra in the potential load calculation is dramatically simplified when the body is fixed. Validation of more general QTFs, including difference frequencies, dichromatic waves, bidirectional waves and body motion, will be given in later sections.

The geometry of the body in this section is very simple, but nevertheless is it remarkable how small the discretisation error is for such a coarse body mesh. In a real analysis of a non-trivial geometry analytic values are unavailable and it is harder to estimate discretisation error, but estimates can be made from a convergence study or by comparing two mathematically equivalent results (see Section 2.5.3). Run times can become very long for large meshes, so using the available error estimates to ensure that your mesh is sufficiently large, but not excessively large, can save significant amounts of time.

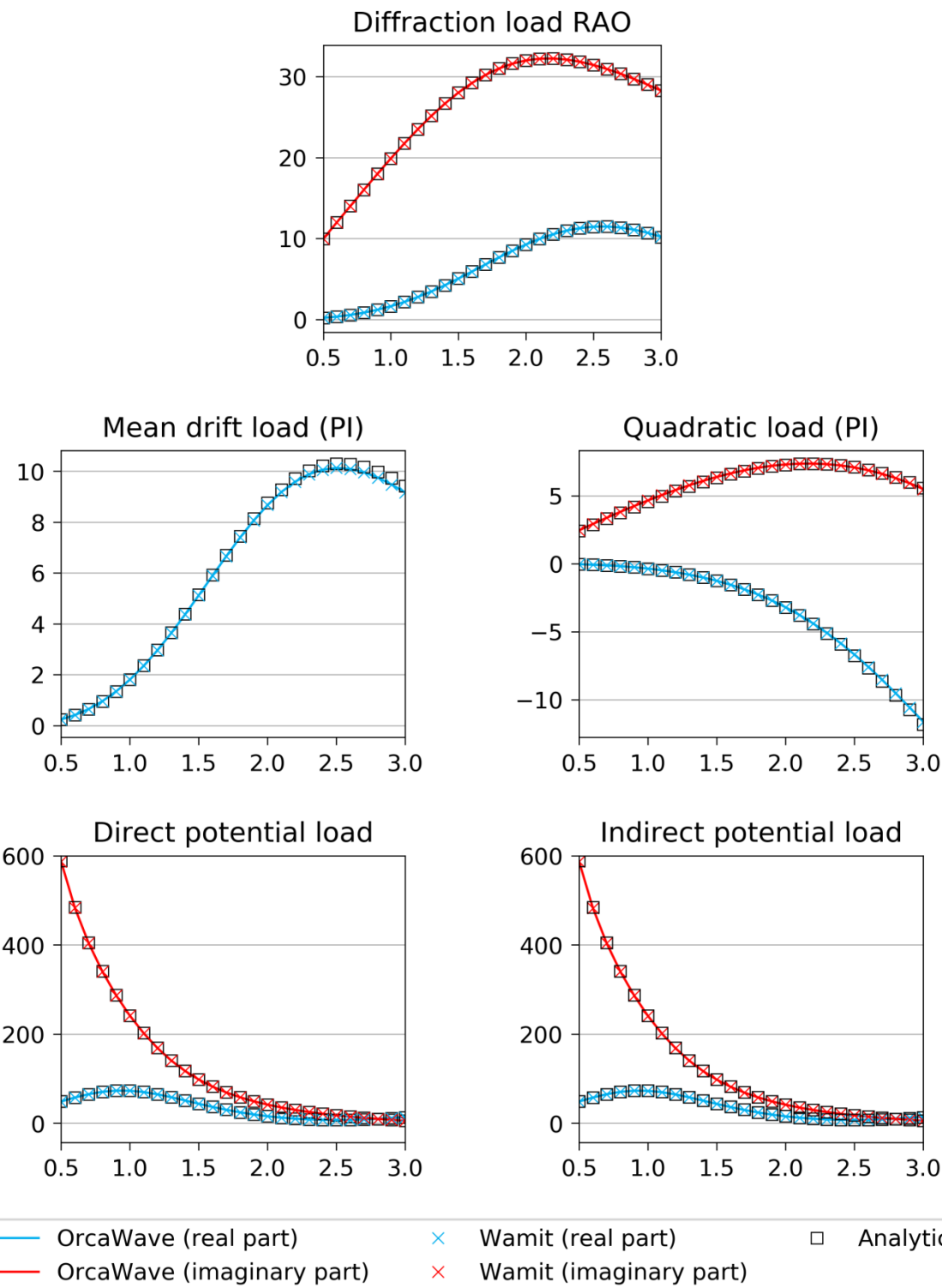


Figure 31. Surge components of: diffraction load RAO (kN/m), mean drift load (kN/m²), sum-frequency quadratic load (kN/m²), sum-frequency direct potential load (kN/m²) and sum-frequency indirect potential load (kN/m²) for the bottom-mounted cylinder. The horizontal axes are angular frequency (rad/s) of the incoming wave.

3.2. QTFs of a floating hemisphere in shallow water

3.2.1. Description

This case is based on the TEST101 case of the Wamit v6.4S program. The body is a freely-floating hemisphere of radius 1m in water of depth 3m. The body mesh file includes panels on the interior free surface for the removal of irregular frequency effects. Two planes of symmetry are used, with a total of 240 panels per quadrant.

For the potential load portion of the QTF calculation a panel mesh of the free surface panelled zone is used that extends to a radius of 3m, using 192 panels per quadrant. A quadrature zone is defined on the free surface for radii $3m \leq r \leq 7m$, and the asymptotic zone is therefore defined by $r \geq 7m$.

The quadratic loads are computed by both PI and CS methods. The control surface is in the shape of a hemisphere and described by a csf file with 80 panels per quadrant.

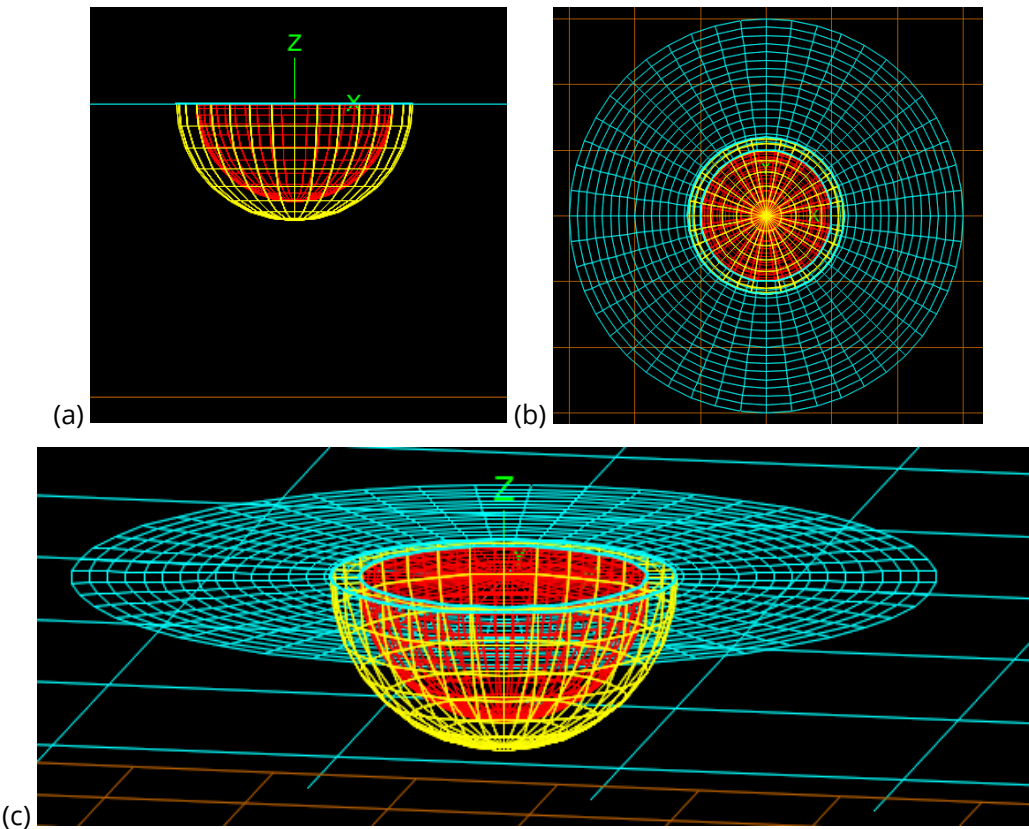


Figure 32. Elevation (a), plan (b) and perspective (c) views of the body mesh (red), control surface mesh (yellow) and the free surface panelled zone mesh (blue).

Following TEST101 of Wamit v6.4S, we evaluate difference frequency QTFs for incident waves with heading $\beta = 0^\circ$. For illustration we choose a single difference frequency of $\omega_2 - \omega_1 = 0.1$ rad/s and consider a range of incident wave frequencies $0.5 \leq \omega_1 \leq 4.5$ rad/s.

3.2.2. Results

Results are shown in Figure 33 for surge force and Figure 34 for heave force. Both show excellent agreement between the programs.

Over most of the frequency range we see close agreement between the PI and CS methods for the quadratic load, indicating that the model is well-resolved by the meshes and the discretisation error is low. As discussed in Section 2.7.3, if other wave headings (e.g. crossing seas) or other degrees of freedom are of interest then those results should also be inspected.

For $\omega \geq 3.5$ rad/s, Figure 33 shows a visible difference in the quadratic surge force between the PI and CS methods. A finer mesh is probably required to analyse these shorter waves. To ascertain which method is giving the most accurate results, the results should be compared to a calculation using a finer mesh – in effect a mini convergence study.

The close agreement between the direct and indirect methods likewise indicates that the calculation of the second-order potential is well resolved and the discretisation error is low. This gives some reassurance, but does not necessarily prove, that the QTF data items in the model all have appropriate values. In particular, a convergence study is required to demonstrate convergence with respect to the *outer radius*, because both methods use the same approximation based on the outer radius to evaluate a free surface integral. In this case the relatively shallow depth of the water ensures that an outer radius of 7m is sufficient [1].

3.2.3. Further considerations

The hemisphere body in this validation case is wall-sided, i.e. it intersects the free surface orthogonally. As noted in Section 2.8.3 and illustrated in Figure 27, we see good agreement between OrcaWave and Wamit results for CS quadratic loads for wall-sided bodies. The quadratic load results in this section are a further example of this.

We have used a different body mesh for the hemisphere in this section to the mesh file used in the Wamit v6.4S test case. The reason we have done so is to ensure that the panels adjacent to the waterline extend to a relatively shallow depth – we have used so-called “cosine spacing” in our mesh. This ensures that the centroid of each waterline panel is relatively close to the free surface, and improves the accuracy of the line integrals around the body waterline that are involved in both the quadratic and potential load calculations. In this case we found that the two meshes gave significantly different quadratic loads at the larger values of ω_1 . To fully assess the level of discretisation error in the results a convergence study would need to be performed.

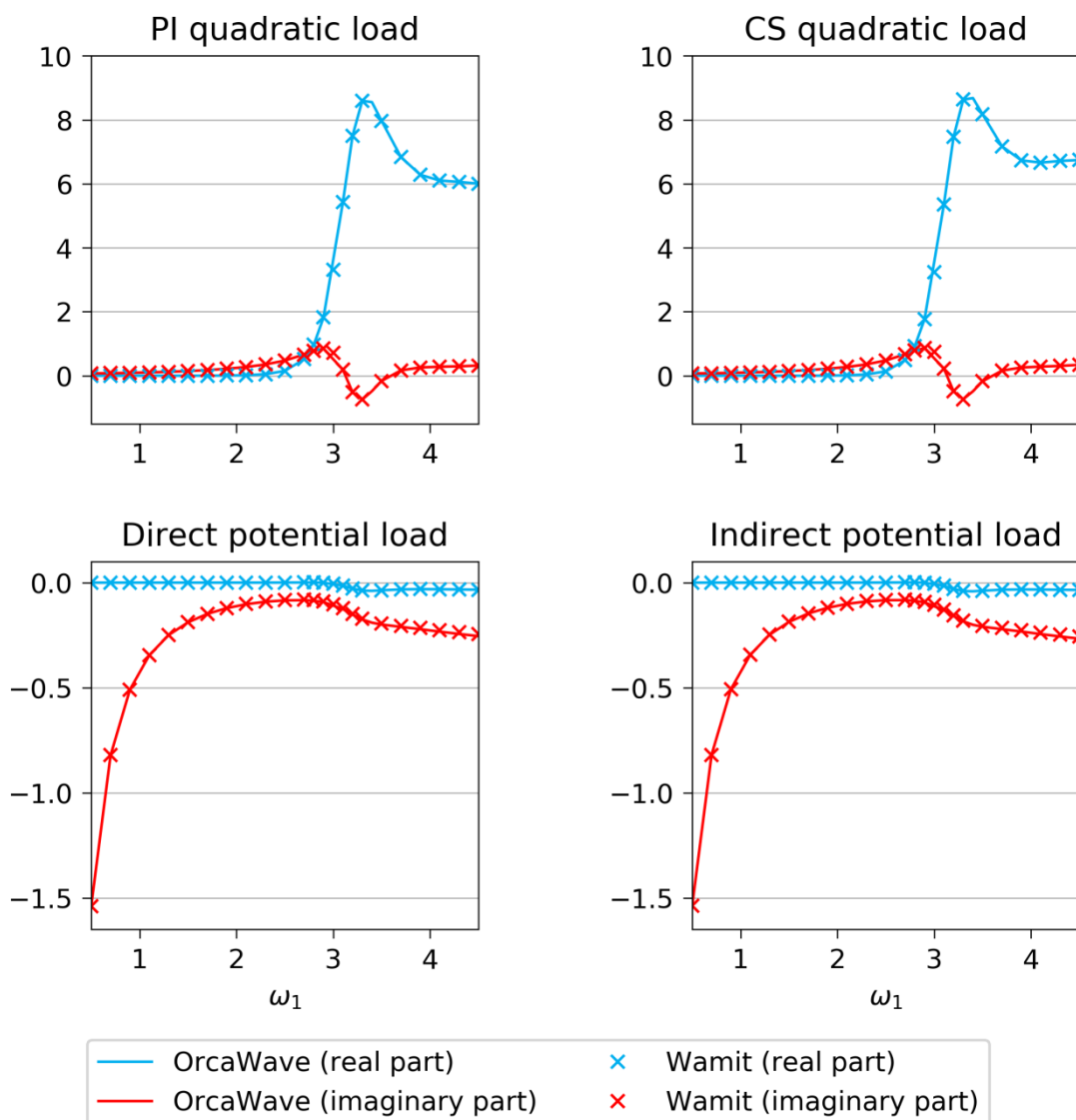


Figure 33. Surge components of the difference-frequency quadratic load and potential load (kN/m²) for $\omega_2 - \omega_1 = 0.1$ rad/s and $\beta = 0^\circ$. The horizontal axes are angular frequency (rad/s) of the longer incoming wave.

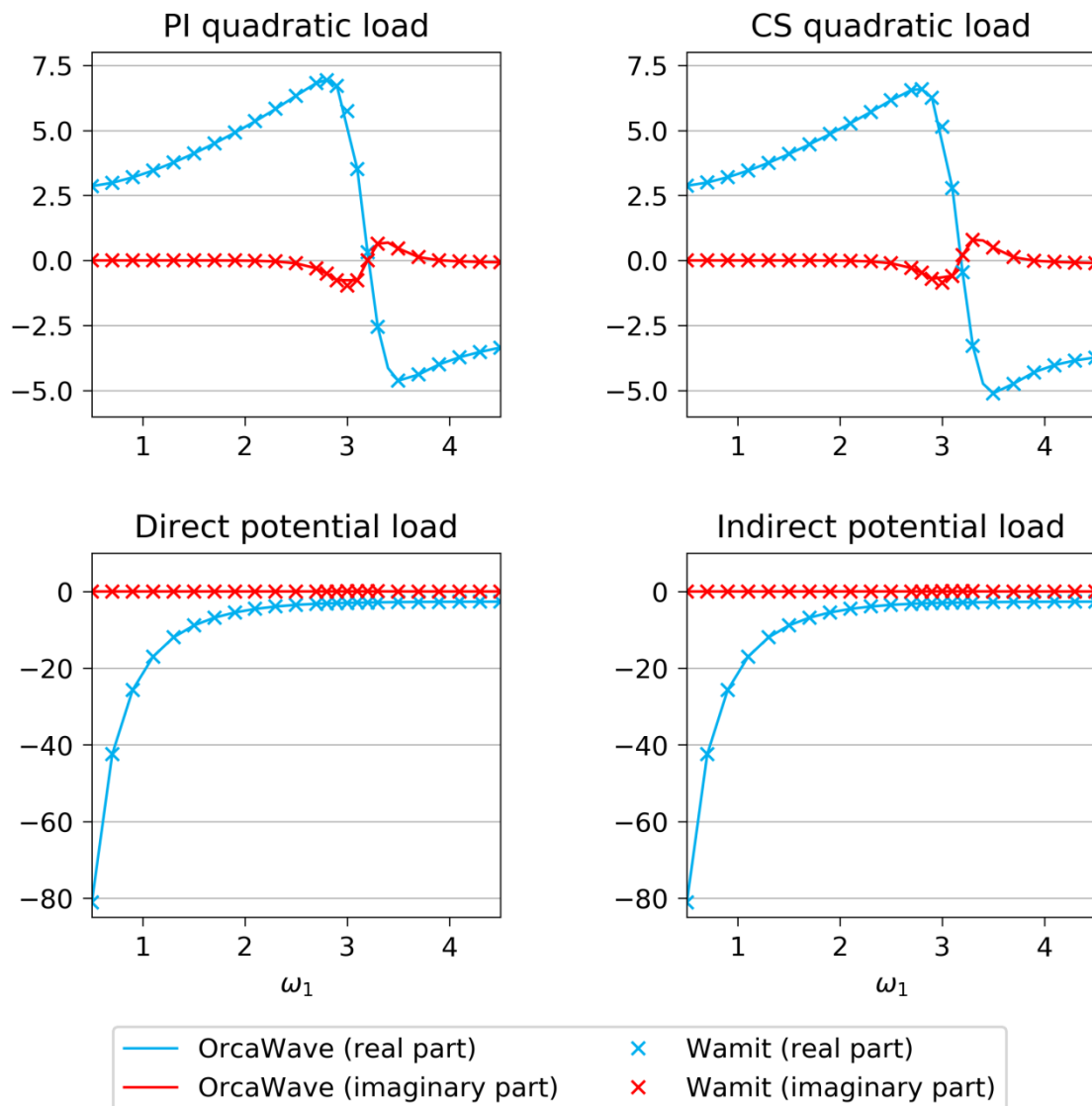


Figure 34. Heave components of the difference-frequency quadratic load and potential load (kN/m^2) for $\omega_2 - \omega_1 = 0.1 \text{ rad/s}$ and $\beta = 0^\circ$. The horizontal axes are angular frequency (rad/s) of the longer incoming wave.

3.3. Multibody QTF analysis of a circular cylinder and ellipsoid

3.3.1. Description

This case is based on the TEST103a case of the Wamit v6.4S program. The same two bodies are present as in Section 2.6, a vertical cylinder which is fixed and an ellipsoid which is freely floating. We use the same position and orientation of the bodies as we did in Section 2.6, so that the global mesh has symmetry in the YZ plane. Note that this differs from the TEST103a case of Wamit v6.4S by a 90° rotation of the entire model – therefore it is fully equivalent, but allows us to make full use of the available symmetry. The water depth is infinite.

Each body mesh has two planes of symmetry and includes panels on the interior free surface for the removal of irregular frequency effects. Instead of using the body mesh files of the Wamit v6.4S test case, we use meshes with finer vertical discretisation in order to improve the accuracy of the second-order forces (as discussed in Section 3.2.3). The cylinder mesh has 420 panels per quadrant and the ellipsoid 220 panels per quadrant.

For the potential load portion of the QTF calculation a panel mesh of the free surface panelled zone is used that extends to a radius of 5m, using 1090 panels per half. No quadrature zone is used, and the asymptotic zone is therefore defined by $r \geq 5\text{m}$.

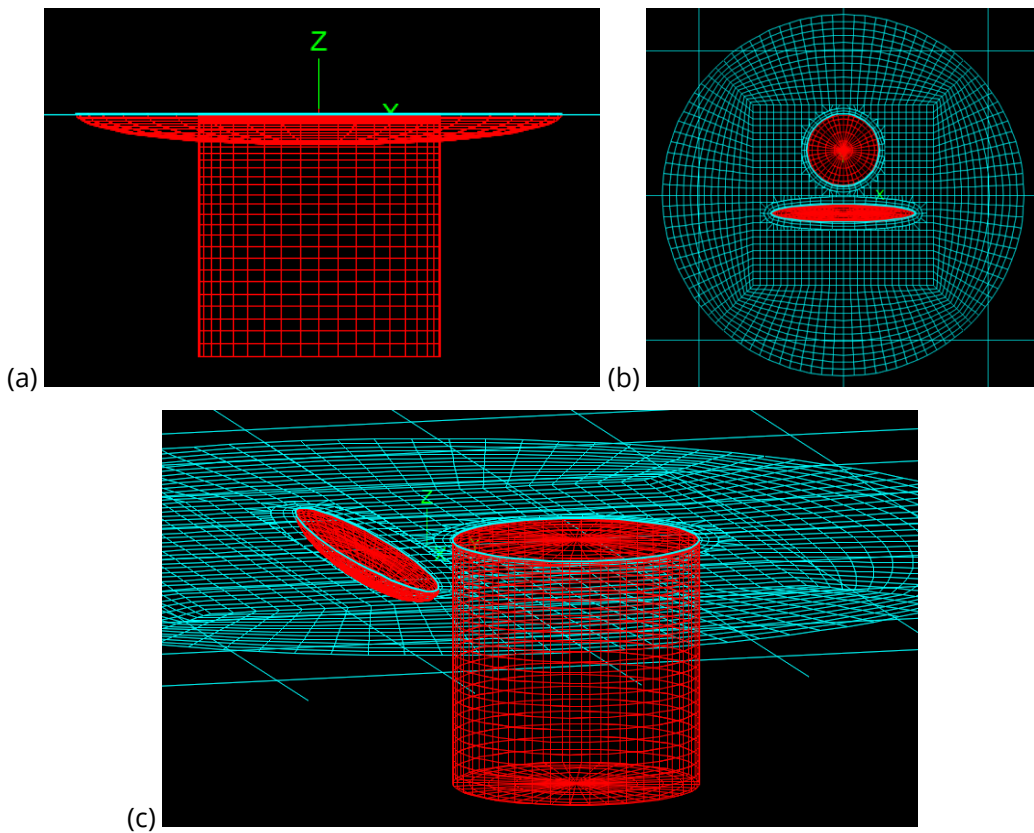


Figure 35. Elevation (a), plan (b) and perspective (c) views of the body meshes of the cylinder and ellipsoid (red) and the free surface panelled zone mesh (blue).

Since we have not yet shown a validation case including bidirectional waves, we consider a range of incident wave headings $\beta = 0^\circ, 30^\circ, 45^\circ, 60^\circ, 90^\circ$. We evaluate difference frequency QTFs for a single difference frequency of $\omega_2 - \omega_1 = 2.5$ rad/s and consider a range of incident wave frequencies $1 \leq \omega_1 \leq 4$ rad/s.

3.3.2. Results

There are many results we could present for this multibody system since there are twelve degrees of freedom in total, six per body. In order to keep the presentation concise we plot the full QTFs, i.e. the sum of the quadratic and potential loads, rather than plotting these components separately as in Sections 3.1 & 3.2.

Figure 36 shows the full QTFs of the cylinder, and Figure 37 the full QTFs of the ellipsoid. We show results for a pair of wave headings $\beta_1 = 0^\circ$, $\beta_2 = 30^\circ$ for the purpose of validating OrcaWave's calculation of bidirectional QTFs. Excellent agreement is seen between the two programs.

The quadratic and potential load components of the QTFs are not plotted separately in this document, but they can be inspected by running the model files that are made available for download. We note that the quadratic and potential loads are of similar magnitude in this case and that, individually, they both show excellent agreement between the two programs similar to the pattern of Figure 36 & Figure 37.

3.3.3. Further considerations

We have not performed a convergence study to estimate the level of discretisation error in the QTF results for this case. We discuss below the issues to consider.

We have used PI quadratic loads in our QTFs, but it is well known that PI quadratic loads are often slow to converge with respect to mesh resolution. The error in these loads could be significant and should be estimated, either by performing a calculation using a finer mesh or by using the same mesh and including CS quadratic loads for comparison.

For the potential loads, a superficially similar procedure is to compare between the direct and indirect methods. However, this only gives limited reassurance because both methods share a key approximation: the outer radius that splits the free surface integral into a panelled zone and an asymptotic zone [1]. This is in strong contrast to the situation for quadratic loads, where the PI and CS methods are so very different that agreement between them is relatively strong evidence that both are well converged. Agreement between direct and indirect potential loads indicates that the body mesh and the panelled zone mesh are sufficiently fine, but does not give any information on whether the outer radius is sufficiently large.

The case studied in this section has infinitely deep water, meaning that the outer radius may need to be significantly larger than it would in shallow water [1, 3]. For this reason, it would be prudent to test convergence of the potential loads by varying the outer radius, even though the direct and indirect potential loads agree well.

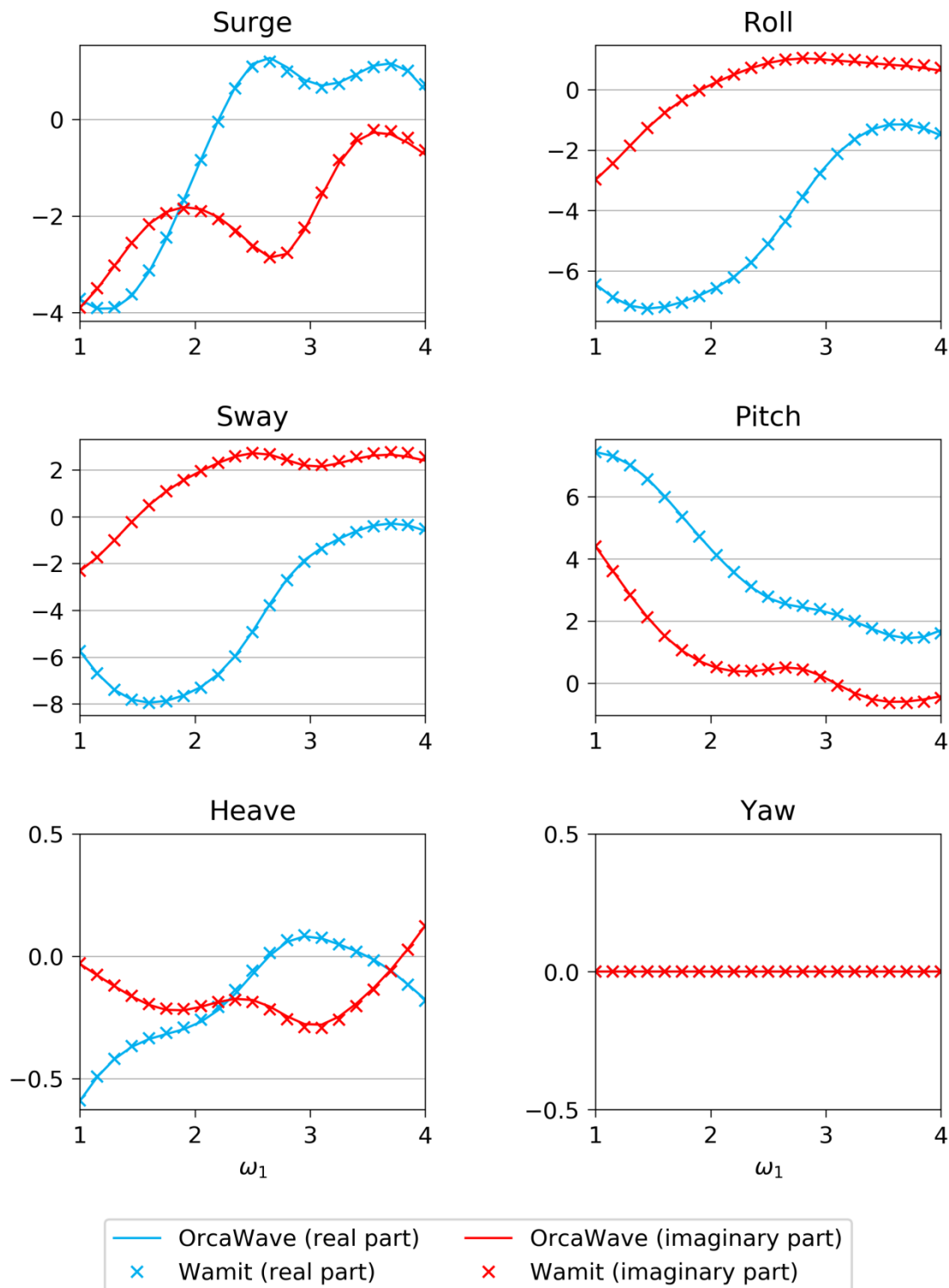


Figure 36. Full QTFs (PI quadratic load plus indirect potential load) for the cylinder. The difference frequency is $\omega_2 - \omega_1 = 2.5$ rad/s, $\beta_1 = 0^\circ$ and $\beta_2 = 30^\circ$. The horizontal axes are angular frequency (rad/s) of the longer incoming wave. The vertical axis is kN/m² for surge, sway and heave, kN.m/m² for roll, pitch and yaw.

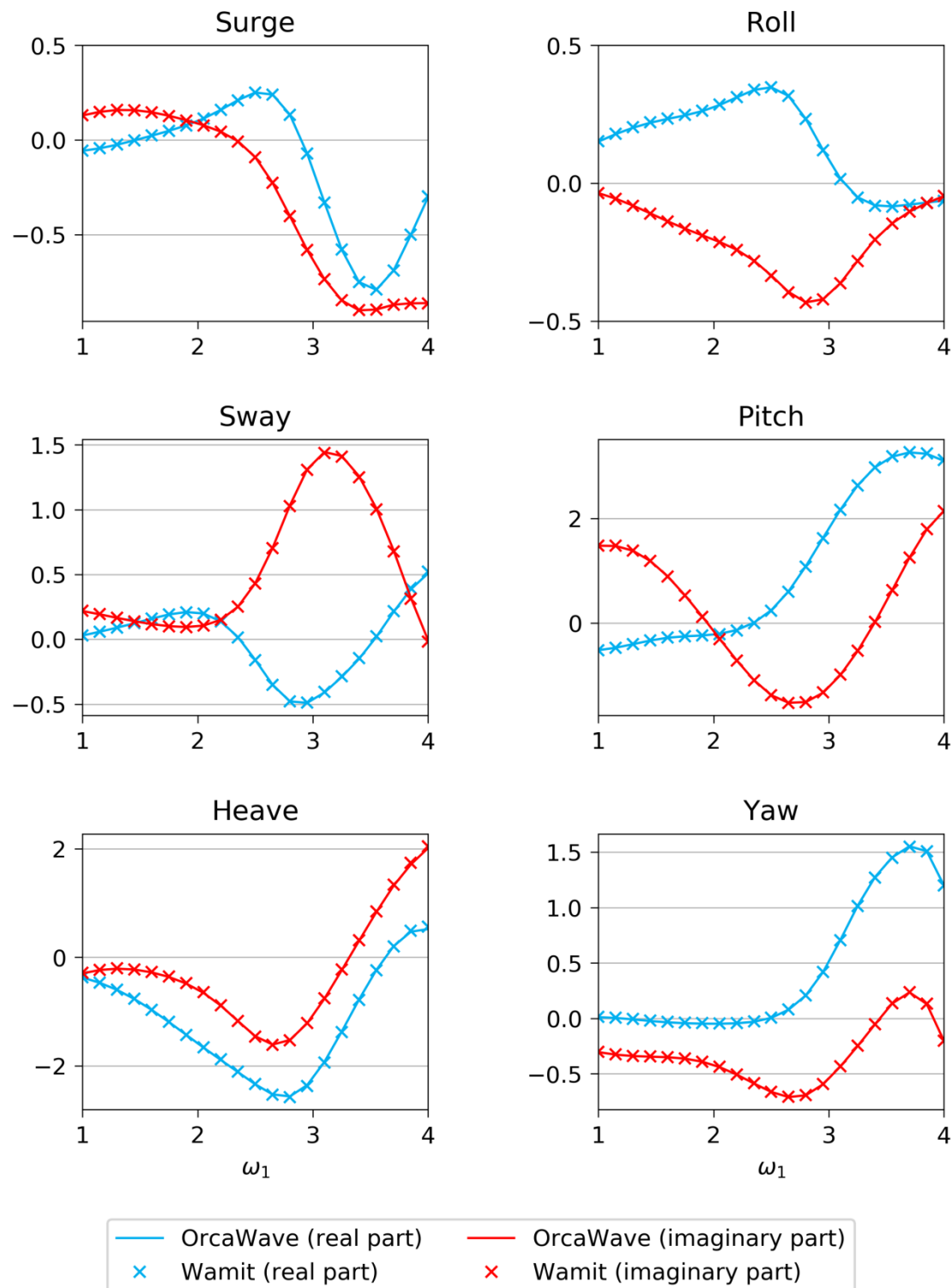


Figure 37. Full QTFs (PI quadratic load plus indirect potential load) for the ellipsoid. The difference frequency is $\omega_2 - \omega_1 = 2.5$ rad/s, $\beta_1 = 0^\circ$ and $\beta_2 = 30^\circ$. The horizontal axes are angular frequency (rad/s) of the longer incoming wave. The vertical axis is kN/m² for surge, sway and heave, kN.m/m² for roll, pitch and yaw.